DEMOCRATIC AND POPULAR ALGERIAN REPUBLIC MINISTRY OF HIGHER EDUCATION AND SCIENTIFIC RESEARCH ECHAHID HAMMA LAKHDAR UNIVERSITY OF EL-OUED FACULTY OF NATURAL SCIENCES AND LIFE DEPARTMENT OF CELLULAR AND MOLECULAR BIOLOGY

Master's thesis

In biological sciences

Specialty: Applied Biochemistry

THEME

Eco-Friendly Synthesis of Copper Oxide Nanoparticles Using *Ephedra alata* from El Oued: Comprehensive Protocols for Biological Applications

Present by: Ben abdallah Saber
Djebloun Ali
Logbi Oualid

Examining committee:

President Tlili Mohamed laïd MCA	El-Oued University
Examiner Boukhari Dalel MAA	El-Oued University
Supervisor Mahboub Nasma **MCA**	El-Oued University
Co-supervisor. Inasse Cherfi	

University year: 2024/2025

Acknowledgment

We would like to express our deepest gratitude to all the individuals who contributed to the success of this thesis .

First and foremost, we extend our sincerest thanks to our thesis supervisor, Mrs. MAHBOUB Nasma, a lecturer at the University of El Oued, for her patience, availability, and especially for her invaluable advice that greatly enriched our thinking throughout this process.

We also wish to warmly thank the entire teaching team at Hamma Lakhdar University, as well as the professional contributors responsible for our training, for ensuring the theoretical aspect of our journey with rigor and competence .

Our heartfelt appreciation goes to our families, parents, brothers, sisters, and friends for their unwavering support and encouragement throughout this project .

We would also like to sincerely thank all the professors, contributors, and every individual who, through their words, writings, advice, and constructive criticism, guided our reflections and kindly agreed to meet with us to answer our questions during our research

Thank you all.

Abstract:

The green synthesis of copper nanoparticles using *Ephedra alata* extract from the El Oued region represents a promising alternative to conventional costly chemical methods, as the biosynthesis approach is environmentally safe. In this study, the nanoparticles were characterized by FTIR spectroscopy, which revealed several functional groups involved in the stabilization of CuNPs, including hydroxyl (–OH) at 3200–3300 cm^{-1}, C–H at 2930 and 2850 cm^{-1}, carbonyl (C=O) at 1750 cm^{-1}, C=C at 1600 cm^{-1}, carboxylate (COO^{-}) at 1400 cm^{-1}, C–N or C–O at 1310 cm^{-1}, ether or polysaccharide vibrations at 1010 cm^{-1}, and a sharp Cu–O bond peak at 600 cm^{-1}, which appeared clearly after calcination of the synthesized material, confirming the successful formation of CuNPs. XRD analysis also showed sharp diffraction peaks at 2θ angles of 38.89° and 35.69°, with corresponding intensities of 1586 and 1505, respectively, indicating the presence of CuO NPs rather than Cu_2O. Cytotoxicity testing showed complete cell death at 20 mg/mL, with an LC_{50} value around 5 mg/mL. The synthesized nanoparticles exhibited promising biological activities, including anti-inflammatory effects reaching 98% at 2.5 g/mL, antibacterial activity against *E. coli* with an inhibition zone of 19 mm at 40 mg/mL, and antifungal effects against *Saccharomyces cerevisiae* with a similar zone of inhibition. The particles also showed notable inhibition of α-amylase starting at 10% at 5 µg/mL and exceeding 80% at 35 µg/mL, indicating potential antidiabetic applications. Furthermore, high antibiofilm activity was recorded, with inhibition rates of 69.64% for *Bacillus* and 67.45% for *Salmonella typhimurium* at the highest tested concentration (900 µg/mL). These findings confirm that the biosynthesis of copper nanoparticles using *Ephedra alata* is a promising strategy for developing nanomedical applications targeting bacteria, fungi, inflammation, and diabetes, while supporting the trend toward sustainable and eco-friendly nanotechnology.

Keywords: Copper nanoparticles, Green synthesis,Sustainable nanotechnology, *Ephedra alata*, Antifungal, Antibacterial, Anti-inflammatory, Antidiabetic, Antibiofilm.

الملخص:

تمثل عملية التصنيع الأخضر لجسيمات النحاس النانوية باستخدام مستخلص Ephedra alataمن منطقة الوادي بديالً واعادا للطرق الكيميائية التقليدية المكلفة، حيث يعد هذا النهج البيولوجي آمانا بيئايا. في هذه الد ارسة، تم توصيف الجسيمات النانوية باستخدام مطيافية الأشعة تحت الحم ارء (FTIR)، والتي كشفت عن وجود عدة مجموعات وظيفية تساهم في تثبيت جسيمات النحاس النانوية (CuNPs)، بما في ذلك مجموعة الهيدروكسيل) – OH عند 3200–3300 سم$^{-1}$)، ومجموعة C–H عند 2930 و2850 سم$^{-1}$، ومجموعة الكربونيل (C=O عند 1750 سم$^{-1}$)، ومجموعة C=C عند 1600 سم$^{-1}$، ومجموعة الكربوكسيلًت (COO^{-}عند 1400 سم$^{-1}$)، ومجموعة C–N أو C–O عند 1310 سم$^{-1}$، واهت از از ت الإيثر أو السكريات المتعددة عند 1010 سم$^{-1}$، بالإضافة إلى قمة حادة ل اربطة Cu–Oعند 600 سم$^{-1}$، والت ي ظهرت بوضوح بعد كلسن ة)حر ق(الماد ة المصنعة، مما يؤكد التكوين الناجح لجسيمات النحا س النانوية. كم ا أظهرت تحاليل حيود الأشع ة السينية) (XRDقمم حيود حادة عند زوايا 2 θبلغت 89.38° و69.35°، بشدات بلغت 1586 و1505 على التوالي، مما يشير إلى وجود جسيمات نانوية من أكسيد النحاس (CuO(بد الا من أكسيد النحاس الأحادي .(Cu$_2$O(أظهرت اختبا ارت السمية الخلوية موتاا خلوايا كامالً عند تركيز 20 ملغم/مل، مع قيمة LC$_{50}$تقدر بحوالي 5 ملغم/مل. كما أظهرت الجسيمات النانوية المصنعة نشاطات بيولوجية واعدة، بما في ذلك تأثي ارت مضادة للَّلتهاب بلغت 98% عند ترك طيز 5.2 غ/مل، ونشا اطا مضاادا للبكتيريا ضد E. coliبمنطقة تثبيط بلغت 19 مم عند 40 ملغم/مل، وتأثي ارت مضادة للفطريات ضد Saccharomyces cerevisiae بمنطقة تثبيط مماثلة. كما أظهرت الجسيمات تثبي اطا ملحو اظا لإنزيم الألفا–أميليز بدأ بنسبة 10% عند تركيز 5 ميكروغ ارم/مل وتجاوز 80% عند 35 ميكروغ ارم/مل، مما يشير إلى تطبيقات مضادة لمرض السكري. بالإضافة إلى ذلك، سُجل نشاط قوي مضاد لتكوين الأغشية الحيوية، حيث بلغت نسب التثبيط 64.69% للبكتيريا Bacillus و45.67% لـ Salmonella typhimurium عند أعلى تركيز تم اختباره) 900 ميكروغ ارم/مل(. تؤكد هذه النتائج أن التخليق الحيوي لجسيمات النحاس النانوية باستخدام Ephedra alata يعد است ارتيجية واعدة لتطوير تطبيقات نانوية طبية تستهدف البكتيريا والفطريات والالتهابات ومرض السكري، مع دعم التوجه نحو تكنولوجيا نانوية مستدامة وصديقة للبيئة.

الكلمات المفتاحية: الإفيد ار الأطا، مضاد للفطريات، مضاد للبكتيريا، مضاد للَّلتهاب، مضاد لمرض السكري، مضاد لتكوين الأغشية الحيوية، جسيمات النحاس النانوية، التخليق الأخضر، نانوتكنولوجيا مستدامة.

List of abbreviations

- $AlCl_3$: Aluminum chloride
- $FeCl_3$: Ferric chloride
- Na_2CO_3: Sodium carbonate
- DPPH: 2,2-diphenyl-1-picrylhydrazyl
- MDA: Malondialdehyde
- GSH: Reduced Glutathione
- TPC: Total Polyphenols Content
- TFC: Total Flavonoid Content
- IC_{50}: Half Maximal Inhibitory Concentration
- EC_{50}: Effective Concentration 50%
- SPF: Sun Protection Factor
- $K_3[Fe(CN)_6]$: Potassium Ferricyanide
- AAs: Ascorbic Acid
- BHT: Butylated Hydroxytoluene
- EEM: Erythemal Effect Spectrum
- GAE: Gallic Acid Equivalents
- mg: Milligrams
- g: Grams
- mL: Milliliters
- AAE: Ascorbic Acid Equivalents
- IC_{50}: Half Maximal Inhibitory Concentration
- min: Minutes
- mIU: Milli-International Units
- L: Liter
- ng: Nanograms
- µg: Micrograms
- RBC: Red Blood Cell
- µL: Microliters
- **FTIR** – Fourier Transform Infrared Spectroscopy
- **UV-Vis** – Ultraviolet–Visible Spectroscopy
- **NPs** – Nanoparticles
- **CuO** – Copper Oxide
- **LC_{50}** – Lethal Concentration 50%
- **SEM** – Scanning Electron Microscopy
- **XRD** – X-ray Diffraction
- **DLS** – Dynamic Light Scattering
- **ZP** – Zeta Potential
- **C=O** – Carbonyl Group
- **C–H** – Carbon–Hydrogen Bond
- **C=C** – Carbon–Carbon Double Bond

- **OH^-** – Hydroxyl Group
- **COO^-** – Carboxylate Group
- **C–N / C–O** – Carbon–Nitrogen / Carbon–Oxygen Bonds
- **Cu–O** – Copper–Oxygen Bond
- **cm^{-1}** – Wavenumber (inverse centimeters)

List of figures

Tables List

summary

CHAPTER II

Nanotechnology

SECOND PART: Experimental Part

CHAPTER I

Materials and Methods

CHAPTER II

Results and Discussion

Introduction

This research addresses the growing global demand for sustainable and eco-friendly nanomaterials by focusing on the biosynthesis of copper oxide nanoparticles. Green nanotechnology still represents a safer and less harmful alternative to conventional chemical methods, as it reduces the release of harmful by-products. In this study, *Ephedra alata* from the El Oued region—a desert medicinal plant native to southeastern Algeria—was used (Karouh et al., 2024; Zaatar et al., 2024).

This plant is rich in alkaloids, various polyphenols, flavonoids, and bioactive compounds that act as both reducing and stabilizing agents during the biosynthesis of nanoparticles.

Traditional methods for synthesizing metal oxide nanoparticles rely on toxic solvents, high energy inputs, and hazardous reducing agents (Ben Amour et al., 2024). These methods pose major risks to the environment and human health. There is a pressing need for safer alternatives capable of producing high-quality nanoparticles without compromising safety. *Ephedra alata* is a promising candidate for such methods due to its rich chemical profile and natural abundance in arid ecosystems (Mew & Nden, 2022; Soultatis et al., 2021).

Additionally, this plant is traditionally used in medicine, pharmaceuticals, and cosmetic treatments. This study stands at the intersection of nanoscience, cellular and molecular biology, environmental engineering, and biomedical sciences. By leveraging the innate biological activity of *Ephedra alata*, the study demonstrates how a locally available plant can be utilized for advanced technological applications.

The synthesized nanoparticles were investigated not only for their catalytic and antibacterial roles but also in terms of their cytotoxicity, biodegradability, and potential use in drug delivery systems. This integrated approach contributes to the global transition toward targeted and sustainable nanomaterials.

The main aim of the study is to develop copper oxide nanoparticles using an environmentally friendly method based on a biologically and medically valuable plant extract. The study explores the functional groups in the plant that contribute to the biosynthesis and stabilization of the nanoparticles. These nanoparticles are then characterized using modern techniques, and their biological functions are evaluated through antibacterial, cytotoxicity, and cellular interaction tests.

> In light of the study's objectives, two central research questions are proposed: Can *Ephedra alata* be effectively used for the green biosynthesis of stable and functional copper oxide nanoparticles? .Do the resulting nanoparticles show potential for applications in biological systems?

FIRST PART

Bibliographic synthesis

CHAPTER I

Ephedra alata

I. Ephedra alata

I.1. Family background

Ephedra alata belongs to the Ephedraceae family, an ancient group of jointed green stems and reduced leaves (Fig. 1). The family is known for gymnosperms that have survived through various climatic shifts. These plants are well-adapted to arid and semi-arid regions, and are often characterized by their
producing ephedrine-type alkaloids, compounds with significant physiological effects (Chroho et al., 2024; Hibi et al., 2022).

Figure 1. Morphological features and habitat of *Ephedra alata* in Algeria (Hibi et al., 2022).

I.2. Ephedra genus background

The genus Ephedra is the sole representative of the family Ephedraceae, comprising approximately 60 species of perennial shrubs (Chroho et al., 2024). These species are mainly distributed in arid and semi-arid regions across Asia, North Africa, the Mediterranean Basin, and the Americas. Ephedra is among the most ancient lineages of gymnosperms, with fossil evidence tracing its origin back to the Early Cretaceous period (approximately 100 million years ago), highlighting its remarkable evolutionary resilience (Wannes & Tounsi, 2023).

I.3. Distribution and habitat

Ephedra alata is native to North Africa and the Middle East, thriving in desert landscapes where few other plants can survive. In Algeria, it is widespread in the El Oued region, where it grows in sandy and rocky soils under extreme temperature and light conditions. Its ability to tolerate salinity and drought makes it a resilient source of bioactive compounds suitable for green chemistry (Chroho et al., 2024; Guo et al., 2023).

I.4. Botanical description

This perennial shrub grows with rigid, green, photosynthetic stems and small, scale-like leaves. It typically reaches up to 60 cm in height and bears small, cone-like reproductive structures.

The stems contain resin canals and are rich in alkaloids and polyphenols, which contribute to the plant's medicinal and ecological value (Dousari et al., 2022).

I.5. Traditional medicinal uses

Ephedra alata has been used in traditional medicine for centuries to treat asthma, bronchitis, fever, and flu. The plant's decoctions are known for their stimulant properties, largely due to ephedrine, and are also used as diuretics and anti-inflammatory agents. In some cultures, it is used to support weight loss and improve respiratory function (Dousari et al., 2022).

I.6. Secondary metabolites

The plant is rich in pharmacologically active secondary metabolites (Bahri et al., 2022; Wannes & Tounsi, 2023). These include:

- **Alkaloids**: Mainly ephedrine and pseudoephedrine, responsible for its stimulant and bronchodilatory effects.
- **Flavonoids**: Such as quercetin and kaempferol, known for their antioxidant and antiinflammatory roles.
- **Tannins and Polyphenols**: Which contribute to antimicrobial and antioxidant activity.

I.7. Biological activities

Ephedra alata's chemical richness translates into diverse biological effects:

I.7.1. Antimicrobial potential

Extracts of the plant have shown significant activity against a variety of Gram-positive and Gram-negative bacteria, as well as fungal strains. These properties are mainly attributed to phenolics and alkaloids that disrupt microbial membranes and metabolic pathways (Zaater et al., 2024).

I.7.2. Anticancer potential

Some studies suggest that the plant's compounds may inhibit the proliferation of cancer cells by inducing apoptosis and interfering with DNA replication. Flavonoids and alkaloids are the likely contributors to these effects, though more research is needed for clinical validation (Sioud et al., 2020).

I.7.3. Antioxidant potential

Due to its high content of polyphenols and flavonoids, *Ephedra alata* exhibits strong antioxidant activity. Its extracts effectively scavenge free radicals, protect cellular components

from oxidative stress, and may reduce age-related cellular damage. In this study (Table 1.), antioxidant capacity was assessed using DPPH, ABTS, and FRAP assays, with results expressed respectively in gallic acid equivalent (GAE), trolox equivalent (TE), and ascorbic acid equivalent (AsE), based on triplicate measurements (n = 3) (Al Jaafreh, 2024).

Table (1). Summarizes the antioxidant activity of *Ephedra alata* ethanol, aqueous, and acetone extracts (Al Jaafreh, 2024).

Extract	DPPH		ABTS		FRAP
	% inhibition	GAE (µg/g)	% inhibition	TE (µg/g)	AsE (µg/g)
Ethanol	70.28 ± 0.74	119	75.85 ± 1.55	70.13	40.75 ± 4.7
Aqueous	90.19 ± 0.58	90	94.17 ± 0.58	75.25	24.86 ± 1.04
Acetone	76.71 ± 0.53	100.1	81.2 ± 1.08	89.3	42.61 ± 2.46

I.7.4. Anti-inflammatory

The traditional use of *Ephedra alata* in managing inflammatory conditions is increasingly supported by scientific evidence. Its bioactive constituents have demonstrated the ability to downregulate key inflammatory markers, suggesting therapeutic potential for disorders such as arthritis, asthma, and skin irritation (Benarba et al., 2021). One commonly used in vitro assay to assess anti-inflammatory potential is the inhibition of albumin denaturation. In this study, the albumin denaturation inhibition activity of *E. alata* extracts was evaluated and expressed as IC_{50} values (µg/ml), calculated from triplicate experiments (n = 3) with standard deviations (Fig. 5) (Al Jaafreh, 2024).

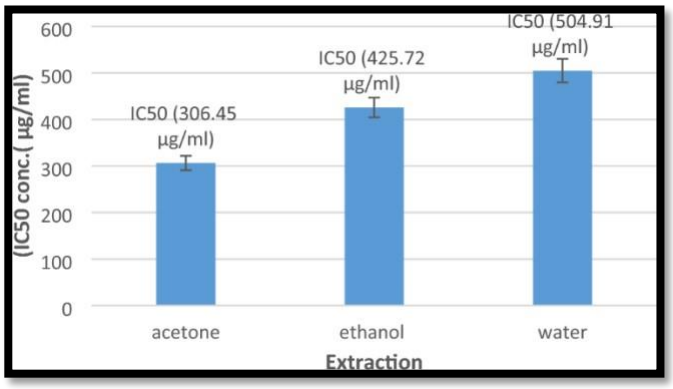

Figure 5. Anti-inflammatory activity of *Ephedra alata* extracts (Al Jaafreh, 2024).

CHAPTER II

Nanotechnology

II. Nanotechnology

Nanotechnology refers to the science, engineering, and application of materials at the nanoscale, which typically ranges from 1 to 100 nanometers. At this scale, materials often exhibit unique physical, chemical, and biological properties not found in their bulk counterparts. These differences arise due to increased surface area-to-volume ratios and quantum effects, making nanomaterials especially reactive and versatile.

The origins of nanotechnology date back to the famous lecture by physicist Richard Feynman in 1959, titled "There's Plenty of Room at the Bottom." However, it wasn't until the 1980s that tools like the scanning tunneling microscope (STM) allowed scientists to manipulate atoms and molecules directly, which opened new doors in materials science, electronics, and biology (Fig. 1).

Nanotechnology has found applications in a wide array of fields, from drug delivery and cancer treatment to water purification, food packaging, and environmental remediation. Its potential lies in its ability to interact with biological systems at the molecular level, enabling highly targeted therapies and efficient biosensors (Fig. 6).

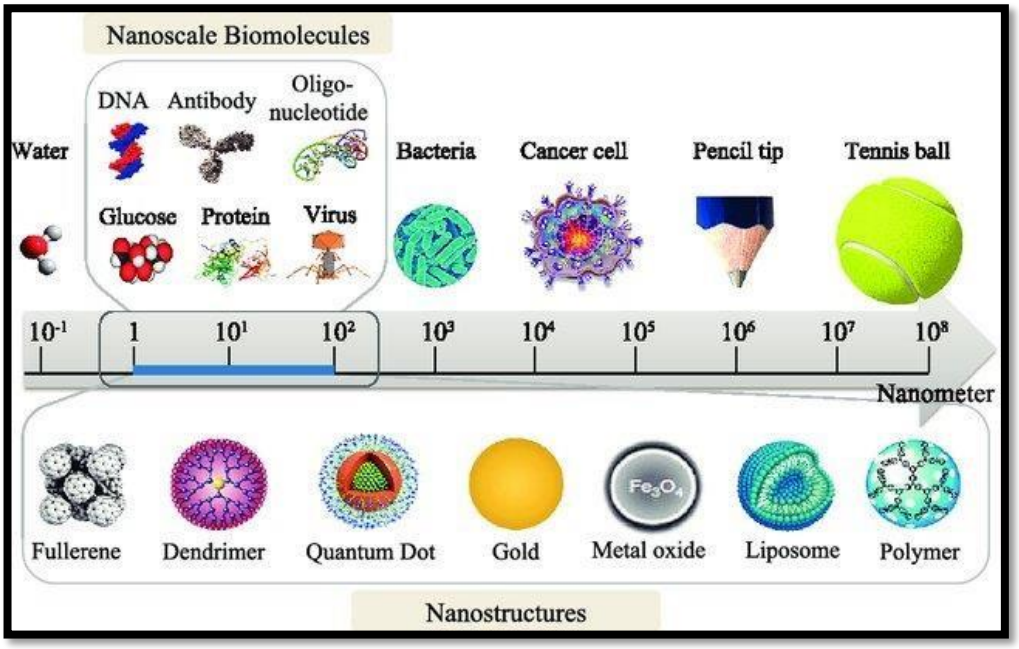

Figure 6. Schematic representation of the nanoscale compared to microscale and macroscale materials (Saallah & Lenggoro, 2018).

II.1. Nanoparticles

Nanoparticles are tiny particles that fall within the 1–100 nm size range. They can be naturally occurring—such as volcanic ash, soot, or virus particles—or synthetically engineered in labs for specific purposes. Because of their high surface-area-to-volume ratio, nanoparticles have enhanced reactivity, strength, and conductivity.

Their size allows them to enter biological systems easily, making them suitable for applications in medicine (e.g., drug carriers), agriculture (e.g., nanopesticides), and electronics (e.g., quantum dots). They are also highly customizable—researchers can coat them with specific molecules to alter their behavior or enhance their compatibility with cells or materials.

Nanoparticles are typically characterized using techniques like Transmission Electron Microscopy (TEM), Scanning Electron Microscopy (SEM), and Dynamic Light Scattering (DLS), each revealing insights about their size, shape, and surface properties.

II.2. Types of nanoparticles

Nanoparticles can be categorized based on their origin, composition, and morphology. A common classification includes organic, carbon-based, and inorganic nanoparticles.

II.2.1. Organic nanoparticles

Organic nanoparticles comprise organic molecules such as lipids, polymers, or proteins. They are generally biocompatible and biodegradable, making them ideal for medical applications, especially drug delivery.

Examples include liposomes (Fig. 8), dendrimers, and micelles. These particles can encapsulate both hydrophilic and hydrophobic drugs and release them at controlled rates in targeted tissues.

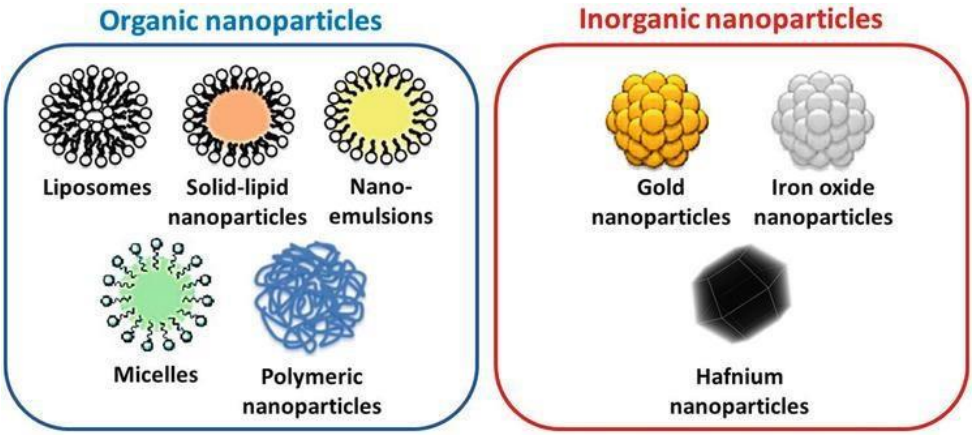

Figure 8. Visual comparison between organic and inorganic nanoparticles, including common types such as liposomes, micelles, gold, and iron oxide nanoparticles (A. Khalil, 2020).

II.2.2. Carbon-based nanoparticles

These include fullerenes, carbon nanotubes, graphene, and carbon quantum dots. Known for their remarkable electrical, thermal, and mechanical properties, carbon-based nanoparticles are used in electronics, biosensors, and energy storage (Fig. 9). They also show promise in photothermal cancer therapy due to their ability to absorb near-infrared light and convert it to heat.

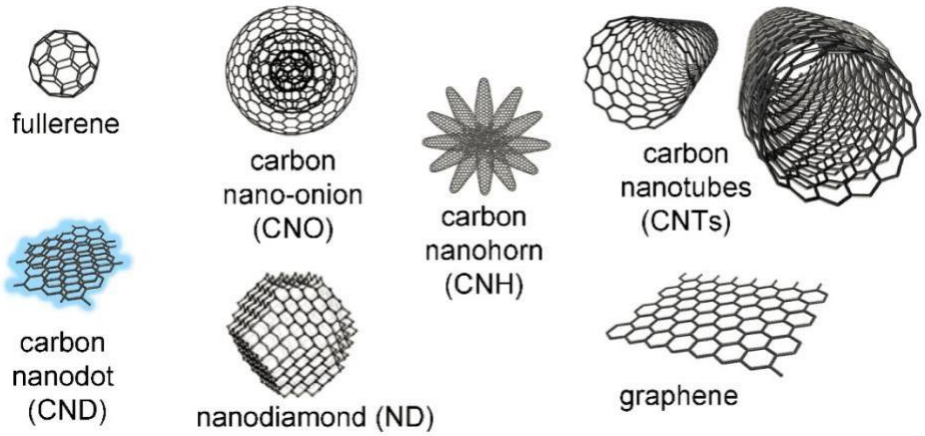

Figure 9. Structural forms of carbon-based nanoparticles (Adorinni et al., 2021).

II.2.3. Inorganic nanoparticles

Inorganic nanoparticles are composed of metals (like gold, silver, copper), metal oxides (like ZnO, TiO_2, CuO), or semiconductors. These are widely used for their antimicrobial, catalytic, and optical properties.

In particular, (Table 2.) copper oxide nanoparticles (CuO NPs) are known for their affordability and multifunctionality, which we'll explore further in the next section.

Table (2). Types of nanoparticles and their typical applications.

Type	Example	Key Application
Organic	Liposomes	Drug delivery
Carbon-based	Graphene	Supercapacitors
Inorganic	CuO	Antibacterial coatings

II.3. Traditional chemical synthesis vs green synthesis

Green synthesis of nanoparticles utilizes natural and non-toxic materials (Table 4.), reduces energy consumption, minimizes waste generation, and promotes environmentally friendly practices (Krahne et al., 2011). It is also more cost-effective and can be easily scaled up for mass production. In contrast, traditional chemical synthesis involves the use of hazardous chemicals, high energy consumption (Fig. 10), the generation of toxic waste, and potential risks to human health and safety (Huston et al., 2021).

Table (03). Key differences between traditional chemical synthesis and green synthesis of nanoparticles.

Aspect	**Traditional Chemical Synthesis**	**Green Synthesis**
Chemicals	Hazardous chemicals	Natural, non-toxic materials (Huston et al., 2021)
Energy consumption	High	Reduced (Huston et al., 2021)
Environmental impact	Pollution, toxic waste	Waste minimization, eco-friendly practices (Singh et al., 2018))
Cost-effectiveness	Expensive	Affordable (Huston et al., 2021)
Scalability	Challenging on a large scale	Adaptable to mass production (Singh et al., 2018)
Health and safety	Potential health and safety risks	Use of non-toxic materials, environmentally friendly processes (Singh et al., 2018)

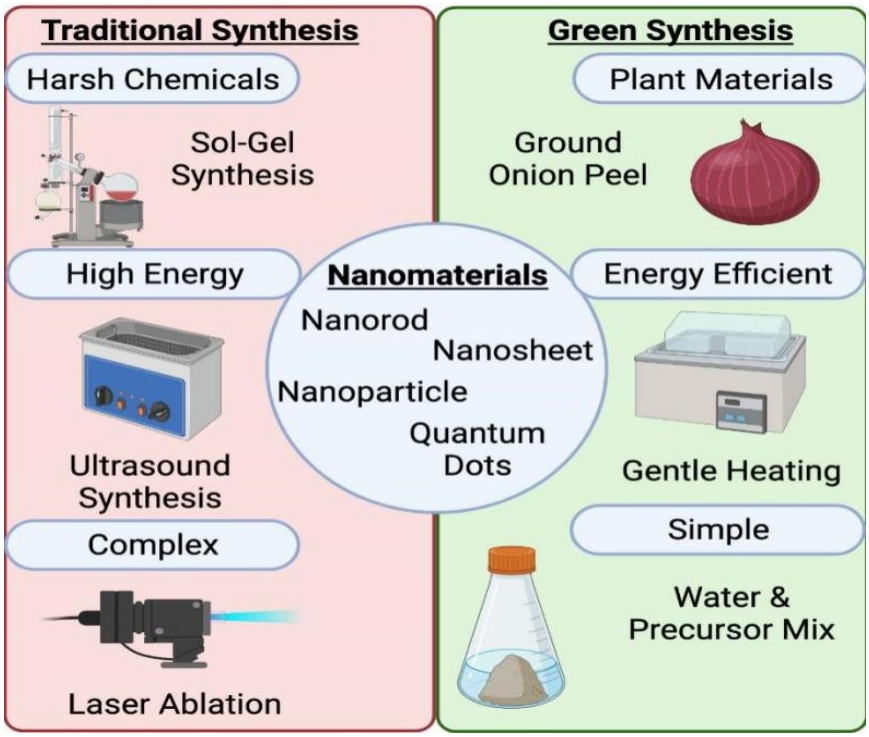

Figure 10. Key differences between traditional chemical synthesis and green synthesis of nanoparticles (Huston et al., 2021).

II.3.1. Advantages of green synthesis of nanoparticles using plant extracts

- **Reduced toxicity**: Chemicals used in traditional synthesis methods can be harmful to the environment and humans. In contrast, plant extracts are generally considered safe and non-toxic.
- **Lower production costs**: Plant extracts are typically less expensive than synthetic chemicals, making green nanoparticle synthesis more cost-effective.

 Enhanced properties: Nanoparticles synthesized using plant extracts may exhibit enhanced properties such as improved antimicrobial and antiviral activity (Dehghani et al., 2023; Sanjivkumar & Silambarasan, 2023).

Green-synthesized nanoparticles using plant extracts have promising applications in agriculture. They can be used as:

- **Antimicrobial agents**: These nanoparticles can effectively combat bacteria, fungi, and viruses that infect crops, improving plant health and reducing yield loss.
- **Nano-environmental fertilizers**: Nanoparticles can enable the slow and controlled release of nutrients into the soil, improving fertilizer efficiency and reducing environmental pollution risks (Jiang et al., 2022).

II.3.2. Disadvantages of green synthesis of nanoparticles using plant extracts

- **Potential harmful effects on plants and soil:**

Despite the advantages, green synthesis of nanoparticles may pose certain drawbacks. For example, a review by Parveen et al. (2023) emphasized that nanoparticle use in agriculture could have detrimental effects on plant and soil health. Additional studies (Parveen et al., 2016) are required to evaluate the long-term environmental and phytotoxic implications of green nanoparticles (Parveen et al., 2023).

II.3.3.Principles of nanoparticle biosynthesis using plant extracts

Biosynthesis of nanoparticles using plant extracts is a green and sustainable approach that leverages bioactive phytochemicals—such as phenolics, terpenoids, and flavonoids—as natural reducing and stabilizing agents. This method offers several advantages, including environmental friendliness, ease of scaling, and the ability to tailor nanoparticle size, shape, and functionality for diverse applications in medicine, catalysis, and nanoelectronics (Jadoun et al., 2021).

As illustrated in (Fig. 11), various plant parts (flowers, fruits, leaves) serve as sources of bioactive compounds. These compounds are typically extracted through maceration, distillation, or rotary evaporation to produce concentrated extracts or essential oils. These plant-derived materials can then be used directly or after modification to synthesize nanomaterials through biologically driven reduction protocols. Depending on the target material and desired nanoparticle characteristics, this process may or may not require heating. The flexibility and low environmental

impact of this approach highlight its growing importance in the field of green nanotechnology (Antunes Filho et al., 2023).

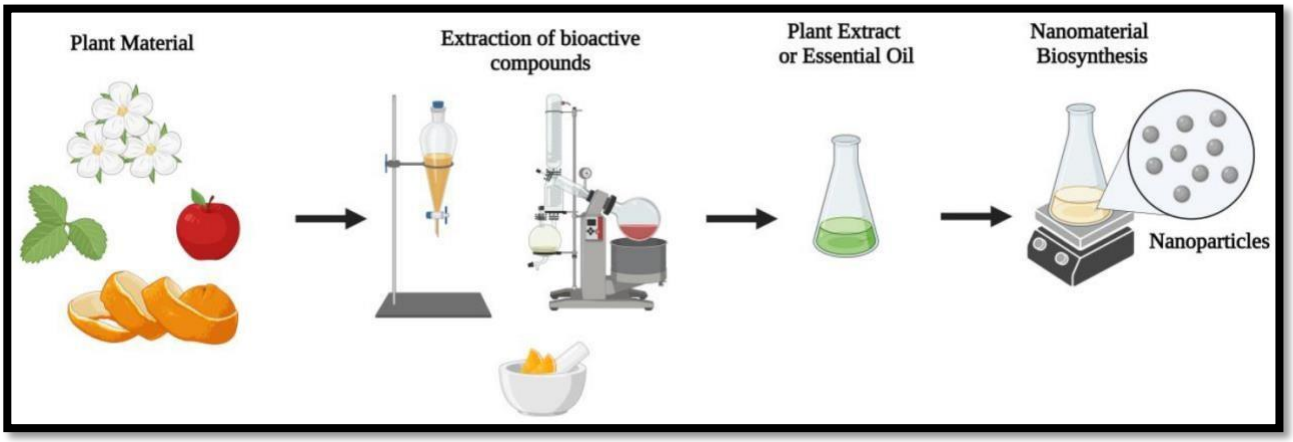

Figure 11. Plant-based extraction for nanoparticle biosynthesis (Antunes Filho et al., 2023).

Ongoing studies aim to further explore biosynthetic mechanisms and potential uses of plant-based nanoparticles (Adeyemi et al., 2022), Among these methods:

A. Reduction Method

- Plant extracts contain phytochemicals such as alkaloids, terpenoids, and phenolic compounds that act as reducing agents.
- Metal ions (e.g., silver, gold, copper) are introduced into the extract solution, and phytochemicals reduce them to nanoparticles.
- This method is simple, cost-effective, and allows precise particle size and morphology control.

B. Complexation Method

- Some phytochemicals in plant extracts can bind to metal ions, forming nanoparticles via complexation.
- This method often yields stable nanoparticles with desirable properties such as catalytic or antimicrobial activity. However, control over particle size and shape may be limited (Miu & Dinischiotu, 2022).

C. Phyto-inspired nanoparticle synthesis

- Researchers study the natural biomolecules in plant extracts involved in nanoparticle formation.
- These insights are used to design synthetic mimetics of such biomolecules for controlled nanoparticle synthesis. While this approach provides better control over particle characteristics, it can be more complex and less sustainable (Zeghoud et al., 2022).

D. Green solvent-mediated synthesis

Conventional nanoparticle synthesis methods often rely on hazardous organic solvents that pose risks to both health and the environment. In contrast, green synthesis approaches emphasize the use of eco-friendly solvents such as water, ethanol, and ionic liquids, which improve the sustainability and environmental safety of the process. A typical green synthesis protocol, (Fig. 12) involves mixing plant extracts rich in phytochemicals like flavonoids, terpenoids, and phenolics with metal ion solutions under controlled temperature and agitation. The reduction of metal ions to metal nanoparticles is usually indicated by a color change in the reaction mixture, which can be further confirmed using UV–visible spectroscopy (Ben Amor et al., 2024; Yazdanian et al., 2022).

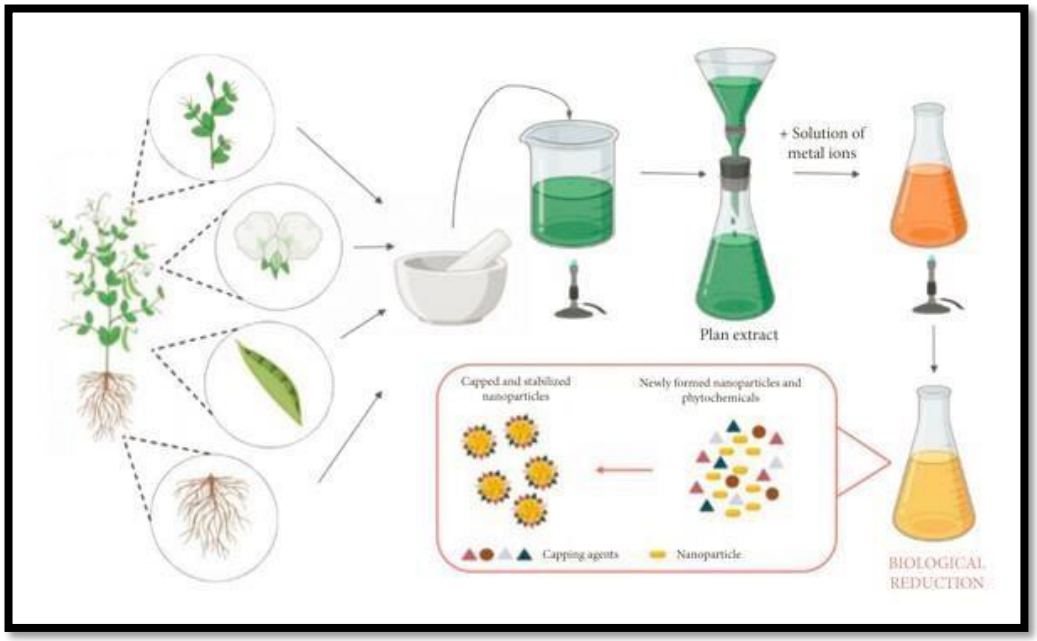

Figure 12. Green synthesis of nanoparticles using plant extracts (Yazdanian et al., 2022).

SECOND PART

Experimental Part

CHAPTER I

Materials and Methods

I. Materials

I.1. Chemicals

A variety of chemical reagents were employed throughout the experimental phases, beginning with the green synthesis of copper oxide nanoparticles (CuO NPs) and extending to the evaluation of their biological activities. Copper(II) sulfate pentahydrate ($CuSO_4 \cdot 5H_2O$) was used as the primary precursor for nanoparticle synthesis, while distilled water served in all stages of sample preparation, dilution, and washing. Whatman Grade 1 filter paper was utilized for filtering the plant extract prior to its reaction. During the in vitro anti-inflammatory assay, egg albumin was used as a protein model to assess protein denaturation inhibition, supported by phosphate-buffered saline (PBS) and sodium hydroxide (NaOH) to maintain and adjust the pH. For antibacterial and antifungal activity testing, Müller-Hinton agar and broth, along with Sabouraud dextrose agar and broth, were used to cultivate bacterial and fungal strains, respectively, and standard antibiotic discs such as gentamicin and amoxicillin served as reference controls. In the biofilm inhibition assay, crystal violet solution (0.1%) was employed to stain the biomass, followed by ethanol or acetone to solubilize the bound dye for quantification. The antidiabetic activity was assessed through the α-amylase inhibition assay using α-amylase enzyme, a starch solution as substrate, and 3,5-dinitrosalicylic acid (DNS) reagent to detect reducing sugars, with NaOH used to adjust the reaction conditions. Hemolytic toxicity testing involved human red blood cells (RBCs) suspended in PBS or 0.9% sodium chloride, while Triton X-100 or DMSO was applied as a positive control for cell lysis. All chemicals were sourced from reliable suppliers, including **Sigma-Aldrich (USA)**, **Pasteur Institute – Algeria**, and **local distributors such as Laboratoire El-Majd**.

I.2. Plant material

The aerial parts of *Ephedra alata* (Ephedraceae) were collected on October 1, 2024, during a field trip to the desert of Hassi Khalifa, located in the northeastern part of El Oued Province, southeastern Algeria. The location of the plant was identified using Google Maps, as previously mentioned. The plant specimen was initially identified based on standard botanical references such as *Flore et végétation du Sahara*, *Nouvelle flore de l'Algérie et des régions désertiques méridionales*, and the African Plants Database, with taxonomic confirmation later provided by specialists. After collection, the aerial parts were shade-dried and then stored in sealed containers at room temperature until use in experimental procedures.

Table (4): Geographic location, collection date, and elevation relative to sea level of the studied plant

Plant	Geographic Coordinates	Region	Collection Date	Elevation Relative to Sea Level
E. alata	33.3572°N, 6.8632°E	Hassi Khalifa, El Oued, Algeria	October 1, 2024	–25 m (below sea level)

I.3. Biological material

The antimicrobial activity of plant materials was evaluated using standard microbial reference strains obtained from the Pasteur Institute of Algeria (Algiers), including American Type Culture Collection (ATCC) strains. The microorganisms tested were taxonomically classified as follows:

- **Gram-positive bacterium**:
  Staphylococcus aureus (ATCC 25932)
  - **Genus**: *Staphylococcus*
  - **Species**: *aureus*
  - **Family**: *Staphylococcaceae*
  - **Phylum**: *Firmicutes*
- **Gram-negative bacteria**:
  Escherichia coli (ATCC 25922)
  - **Genus**: *Escherichia*
  - **Species**: *coli*
  - **Family**: *Enterobacteriaceae*
  - **Phylum**: *Proteobacteria*

  Klebsiella pneumoniae (ATCC 13883)

  - **Genus**: *Klebsiella*
  - **Species**: *pneumoniae*
  - **Family**: *Enterobacteriaceae*
  - **Phylum**: *Proteobacteria*

  Pseudomonas aeruginosa (ATCC 27853)

  - **Genus**: *Pseudomonas*
  - **Species**: *aeruginosa*
  - **Family**: *Pseudomonadaceae*
  - **Phylum**: *Proteobacteria*
- **Yeasts (unicellular fungi)**:
  Candida albicans (ATCC 10231)
  - **Genus**: *Candida*
  - **Species**: *albicans*

- **Family**: *Saccharomycetaceae*
- **Phylum**: *Ascomycota*

Saccharomyces cerevisiae

- **Genus**: *Saccharomyces*
- **Species**: *cerevisiae*
- **Family**: *Saccharomycetaceae*
- **Phylum**: *Ascomycota*

- **Filamentous fungus**:
  Penicillium chrysogenum
  - **Genus**: *Penicillium*
  - **Species**: *chrysogenum*
  - **Family**: *Trichocomaceae*
  - **Phylum**: *Ascomycota*

II. Methods

II.1. Preparation of the extracts of plant material

The aerial parts of *Ephedra alata* were thoroughly washed with distilled water to remove dust and debris, then shade-dried at room temperature and ground into a fine powder. A quantity of 50 g of the powdered plant material was infused in 500 mL of warm distilled water at 40°C. The extraction process was carried out by maceration (Harborne, 1998)[1], with occasional stirring every hour for a total duration of 24 hours. After extraction, the mixture was filtered using Whatman No. 1 filter paper to remove any solid residues. The filtrate was then stored at 4°C for further use in nanoparticle synthesis. The yield of the extract was approximately 10%, calculated based on the dry weight of the extract relative to the initial plant material.

Figure 13. Original photo taken by the research group during fieldwork (2025 ***Ephedra alata*** **Plant in the El Oued Region, 10 km Northeast of Hassi Khalifa, in a Pristine Desert Area**

The yield of the extracts was determined using the following formula (Harborne, 1998) modified by Chouikh *et al.* 2015 (Atef et al., 2015) :

Yield (%) = (W_1 / W_2) x 100 (Equation 1) where:

- W_1 = weight of the extract dried (g).
- W_2 = weight of the plant starting material (g).

II.2. Detection of Functional Groups in *Ephedra alata* Extract by FTIR Analysis

Fourier Transform Infrared (FTIR) spectroscopy is a powerful technique used to identify the functional groups present in plant extracts, which are critically involved in the biosynthesis and stabilization of copper nanoparticles. The process begins with the drying of the aerial parts of the plant, followed by extract preparation using an appropriate solvent such as distilled water, or by using the plant material in its dry powdered form. The sample is then subjected to FTIR analysis within a spectral range of 4000 to 400 cm^{-1}. Characteristic absorption peaks corresponding to functional groups such as hydroxyl (-OH), carbonyl (C=O), and amine ($-NH_2$) are typically observed. These groups are primarily responsible for reducing Cu^{2+} ions and stabilizing the formed nanoparticles.

II.3. Green synthesis of CuO nanoparticles using *Ephedra alata* extract

The student researchers carried out the green synthesis of copper oxide nanoparticles using an aqueous extract of *Ephedra alata*. This extract acts simultaneously as a reducing and stabilizing agent, following an eco-friendly pathway that aligns with the principles of sustainable nanotechnology (Atri et al., 2023).

The students mixed the aqueous extract of *Ephedra alata* with copper(II) sulfate pentahydrate and sodium hydroxide solution (1 M), while preparing the necessary equipment including a pH meter, a magnetic stirrer with a heater, a centrifuge, a drying oven, and an electric furnace for calcination. ئ

To prepare the copper precursor solution, 1 gram of $CuSO_4 \cdot 5H_2O$ was dissolved in 100 mL of distilled water to obtain a 0.1 M solution. Then, 50 mL of the plant extract was added to this solution with continuous stirring using a magnetic stirrer. Simultaneously, the pH of the mixture was adjusted to 10 using 1 M NaOH, since alkaline conditions promote the formation of copper oxide nanoparticles.

The mixture was then heated to a temperature ranging from 60 to 80 °C with continuous stirring for a period of 2 to 4 hours. A visible color change from light blue to dark brown was observed, indicating the reduction of Cu^{2+} ions and the formation of nanoparticles.

After allowing the mixture to cool to room temperature, centrifugation was performed at 5000 rpm to separate the nanoparticles. The resulting particles were washed with distilled water and ethanol to remove impurities, then dried in an oven at 60 °C for 12 hours. Finally, calcination was carried out at 550 °C to obtain a fine, pure, and crystalline black CuO nanopowder.

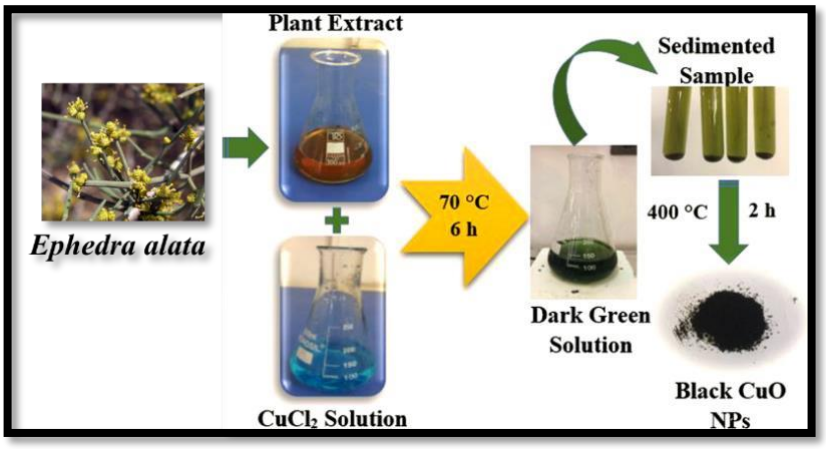

FIGURE 14. Original schematic diagram designed by the student research group (2025)
Schematic Diagram of CuO-NPs Synthesis from *Ephedra alata* to Black Powder Formation

II.4. Physicochemical Characterizations

II.4.1. UV-Visible Spectrophotometry Analysis (UV-Vis)

The spectrophotometer is an instrument that uses a light source to emit polychromatic radiation in the UV-visible and near-infrared range (200–800 nm). This radiation passes through a monochromator (Fig. 16) to become monochromatic. The beam is then split into two: one passes through the sample to be analyzed, and the other through a reference sample. Both beams then reach a detector, which converts the light into an electrical signal. This signal is transmitted to a recorder, allowing absorbance curves to be plotted as a function of wavelength (Passos & Saraiva, 2019).

The UV-Vis absorption spectra of CuO NPs were recorded in the wavelength range of 200 to 800 nm, with a spectral resolution of 1 nm. The obtained data allowed the identification of the wavelengths corresponding to the maximum absorption peaks. The bandgap energies were calculated using the equation:

$$E = \frac{hc}{\lambda}$$

where h is Planck's constant, c is the speed of light, and λ is the wavelength at the peak maximum. The calculated energy was found to be 3.13 Ev (Akash et al., 2020; Passos & Saraiva, 2019).

II.4.2. FTIR Analysis

Fourier-transform infrared spectroscopy (FTIR) is an analytical technique based on the absorption of infrared light by the molecules of a sample. When an infrared beam passes through the sample, specific frequencies are absorbed depending on the characteristic vibrations of the chemical bonds present. These absorptions are unique to each functional group, enabling their identification. The FTIR spectrometer uses an interferometer to generate a modulated signal, which is then transformed into an absorption spectrum using a Fourier transform algorithm. The resulting spectrum displays the absorption intensity as a function of wavenumber (cm^{-1}), providing detailed information on the chemical composition and molecular structure of the sample. This technique is widely used for both qualitative and quantitative analysis of organic and inorganic materials (Franca & Oliveira, 2022; Wenning & Scherer, 2013).

The infrared spectra were recorded in the spectral range of 4000 to 400 cm^{-1}, with a resolution of 4 cm^{-1}. Powdered samples of CuO nanoparticles were analyzed to identify characteristic Cu–O bond vibrations, as well as any shifts related to phytochemical capping or stabilizing agents present in the *Ephedra alata* extract (Wenning & Scherer, 2013).

II.4.3. XRD analysis

X-ray diffraction (XRD) analysis was employed to determine the crystalline structure of the synthesized copper oxide nanoparticles. The analysis was performed using an X-ray diffractometer equipped with Cu-Kα radiation (λ = 1.5406 Å). The diffraction pattern was recorded over a 2θ range of 10° to 80°. The obtained peaks were compared with standard JCPDS data to confirm the phase and purity of the nanoparticles.

II.5 Biological activities in vitro

II.5.1 Cytotoxicity assay

The effect of a nanoparticle solution on the growth of *Saccharomyces cerevisiae* was assessed using a growth sensitivity and cytotoxicity assay. A stock solution of the nanoparticle suspension was prepared at an initial concentration of 20 mg/mL and then serially diluted two-fold to obtain final concentrations ranging down to 0.625 mg/mL. Yeast cells were adjusted to a concentration of 2×10^7 cells/mL in 100 mM potassium phosphate buffer (pH 7) and treated with the nanoparticle solution at various concentrations in a 96-well plate. The mixture was incubated at 37°C for 30

minutes, and untreated cells were used as a negative control to evaluate the effect of the nanoparticles on yeast growth.

For a semi-quantitative spot-test, 2.5 µL of each treated culture from the 96-well plate was spotted onto solid YPD-agar plates containing 2% glucose, both with and without the nanoparticles at the corresponding concentrations. The plates were incubated at 37°C for 48 hours, and after incubation, yeast growth was documented using an Epson® scanner. The growth of treated samples was compared to the untreated control, allowing for an assessment of the cytotoxic or inhibitory effects of the nanoparticles at different concentrations (Ben Amor et al., 2024).

II.5.2. anti–inflammatory activity

This protocol investigates the denaturation of proteins using egg white as a model system and assesses the inhibitory effects of PNs in vitro. With slight modifications for utilizing smaller volumes in a microplate assay, a 10% solution of egg white proteins is prepared by diluting the egg white in distilled water. 50 µL of the egg white solution is added to each well of the microplate, along with 10 µL of the PNs Different concentrations of CuO nanoparticles (1.25, 2.5, 5, 10, 20, and 40 mg/mL) The mixture is incubated at a temperature of 70-80°C for 15-20 minutes.

The extent of protein denaturation is measured by UV-Visible spectrophotometry at 280 nm. Aspirin is used as a reference at different concentrations to evaluate its effects on protein denaturation under the same conditions. The original protocol has been adjusted to use a total volume of 60 µL per well, optimizing material use and improving the assay's efficiency in a microplate format.

Calibration curves for both egg white proteins and aspirin are generated to quantify the results. The ability of the plant extract to inhibit protein denaturation is compared to aspirin using absorbance data, allowing for the evaluation of its potential protective effects (Chaiya et al., 2022; Chandra et al., 2012; Dharmadeva et al., 2018; Elias & Rao, 1988).

The percentage inhibition of protein denaturation will be calculated by:

$$\% \text{ Inhibition} = \frac{Absorbance\ of\ control - Absorbance\ of\ Sample}{Absorbance\ of\ Control} \times 100 \quad \text{(Equation 5)}$$

II5.3. Antibacterial activity

The disk diffusion method is the gold standard for confirming the susceptibility of bacteria. Standardized disk diffusion was introduced by Bauer and Kirby's experiments in 1959 (Bauer et al., 1959), Presently, the Clinical and Laboratory Standards Institute (CLSI) has issued multiple accepted and approved standards for bacteria and yeast testing (Barry, 2007). This study used the widely used method for evaluating the antimicrobial activity of plant or microbial extracts is the well-agar diffusion method. This method follows a procedure similar to the disc spread method, in which the volume of microbial inoculum is spread across the entire surface of the agar plate (Silva et al., 2013).

The antibacterial activity of the compound was assessed using the well diffusion method (WD) against four bacterial strains: *Candida albicans* ATCC 10231 and bacterial strains, including two Gram-negative strains, *Pseudomonas aeruginosa* ATCC 27853, and *Escherichia coli* ATCC 25922, and two Gram-positive strains, *Staphylococcus aureus* ATCC 25923 and *Bacillus subtilis* ATCC 25973.. The compound was prepared at concentrations of 5 mg/mL and 10 mg/mL in DMSO. Mueller-Hinton agar was used as the growth medium. The bacterial strains were cultured on agar plates and incubated at 37°C for 24 hours. To ensure a consistent inoculum size, the bacterial cultures were mixed with 0.9% NaCl solution and adjusted to a turbidity equivalent to McFarland 0.5 standard ($10^{\wedge 8}$ CFU/mL) (Fig 15).

.

Figure 15: Original photo taken by the research group (2025), showing the tools used in the antibacterial activity test.

Subsequently, the agar was poured into Petri dishes, and the bacterial suspension was swabbed evenly onto the agar surface. Wells with a diameter of 6 mm were created in the agar, and 50 µL of the compound at the respective concentrations were added to each well. The plates were

then incubated at 37°C for 24 hours. The experiment was performed in triplicate to ensure accuracy and reproducibility. The zone of inhibition observed around the wells indicated the antibacterial activity of the different extracts of *B. oleracea* against the tested bacterial strains.

II.5.4. Antidiabetic activity

This protocol outlines the evaluation of alpha-amylase activity in the presence of nanoparticle solutions (PNs) using a microplate and iodine assay technique. The assay involves preparing a reaction mixture in each well of a 96-well microplate, where 40 µL of a 1% w/v starch solution (substrate) is combined with 40 µL of nanoparticle solution (PNs) at varying concentrations and 20 µL of a pre-diluted alpha-amylase enzyme solution. The mixture is incubated at 37°C for 10 minutes to allow the enzyme to interact with the starch in the presence of the nanoparticle solutions. After incubation, the reaction is stopped by adding 20 µL of iodine reagent, which forms a blue-black complex with any undigested starch. Controls are included to ensure accurate results: a negative control where starch and enzyme are present without any PNs, and a positive control where starch and enzyme are present with no iodine reagent. Additionally, acarbose, a known alpha-amylase inhibitor, is used as a reference to establish a baseline for enzyme inhibition. Absorbance of the iodine-starch complex is measured at 620 nm using a plate reader, where higher absorbance indicates more undigested starch, reflecting reduced enzymatic activity. The data obtained allows for the comparison of the inhibitory effects of the nanoparticle solutions with the known efficacy of acarbose, providing a clear measurement of their potential as alpha-amylase inhibitors (Chakrabarti et al., 2014; Granados-Guzmán et al., 2022; Khadayat et al., 2020).

II.5.5. Antifungal activity

This protocol outlines the application of the agar well diffusion method to assess the antifungal activity of polymeric nanoparticles (PNs) against *Saccharomyces cerevisiae* and *Penicillium chrysogenum*.

Sterile Petri dishes were prepared with Sabouraud dextrose agar (SDA) supplemented with 2% glucose. Each plate was aseptically inoculated with standardized fungal suspensions. For *S. cerevisiae*, suspensions were adjusted to a 0.5 McFarland standard (~1.5×10^8 CFU/mL) using the VITEK® DENSICHEK® system. Similarly, *P. chrysogenum* conidial suspensions were prepared to the same turbidity standard.

The fungal suspensions were uniformly spread over the agar surface using sterile cotton swabs. After surface drying, uniform wells (~6 mm diameter) were created using sterile Pasteur

pipettes. Each well was then loaded with 50 µL of PNs at different concentrations (40, 20, 10, and 5 mg/mL).

Plates inoculated with *P. chrysogenum* were incubated at 28°C, while those with *S. cerevisiae* were maintained at 37°C, both for 48–72 hours. Antifungal efficacy was evaluated by measuring the diameter of the clear inhibition zones surrounding each well. A zone of inhibition >6 mm was considered indicative of antifungal activity (Magaldi et al., 2004; Tran et al., 2022).

or inhibitory effects of the nanoparticles at different concentrations (Ben Amor et al., 2024).

II.5.6. Antibiofilm Activity Protocol

To assess the antibiofilm activity of copper oxide (CuO) nanoparticles synthesized from *Ephedra alata*, the following protocol is followed:

- **Preparation of Bacterial Suspension**: Prepare bacterial cultures of *Bacillus subtilis* and *Salmonella typhimurium* in nutrient broth and incubate at 37°C until they reach the mid-log phase. Adjust the bacterial suspension to 10^8 CFU/mL using a 0.9% NaCl solution.
- **Preparation of Nanoparticles**: Prepare a series of CuO nanoparticle concentrations ranging from 100 µg/mL to 900 µg/mL by dissolving the nanoparticles in sterile distilled water or DMSO.
- **Biofilm Formation**: Add 200 µL of bacterial suspension to each well of a 96-well microplate. Then, add 50 µL of CuO nanoparticle solution to the corresponding wells. Incubate the plate at 37°C for 24 hours to allow biofilm formation.
- **Biofilm Staining**: After incubation, remove the bacterial suspension and wash the wells three times with phosphate-buffered saline (PBS) to remove non-adherent bacteria. Stain the biofilm by adding 200 µL of 0.1% crystal violet solution to each well and incubate for 15 minutes at room temperature.
- **Washing and Measurement**: Remove the crystal violet solution and wash the wells with PBS to remove excess dye. To quantify the biofilm, add 200 µL of 95% ethanol to each well to dissolve the crystal violet stain. Measure the absorbance at 570 nm using a microplate reader.
- **Calculation of Inhibition**: The percentage of biofilm inhibition is calculated using the formula:

$$\text{Inhibition } \% = ((\text{A control} - \text{A sample})/\text{Acontrol}) \times 100$$

Where AcontrolA_{\text{control}} is the absorbance of the control well (without nanoparticles), and AsampleA_{\text{sample}} is the absorbance of the well treated with CuO nanoparticles.This protocol provides a detailed procedure for evaluating the antibiofilm activity of CuO nanoparticles and can be adapted for different bacterial strains or nanoparticle concentrations as needed.

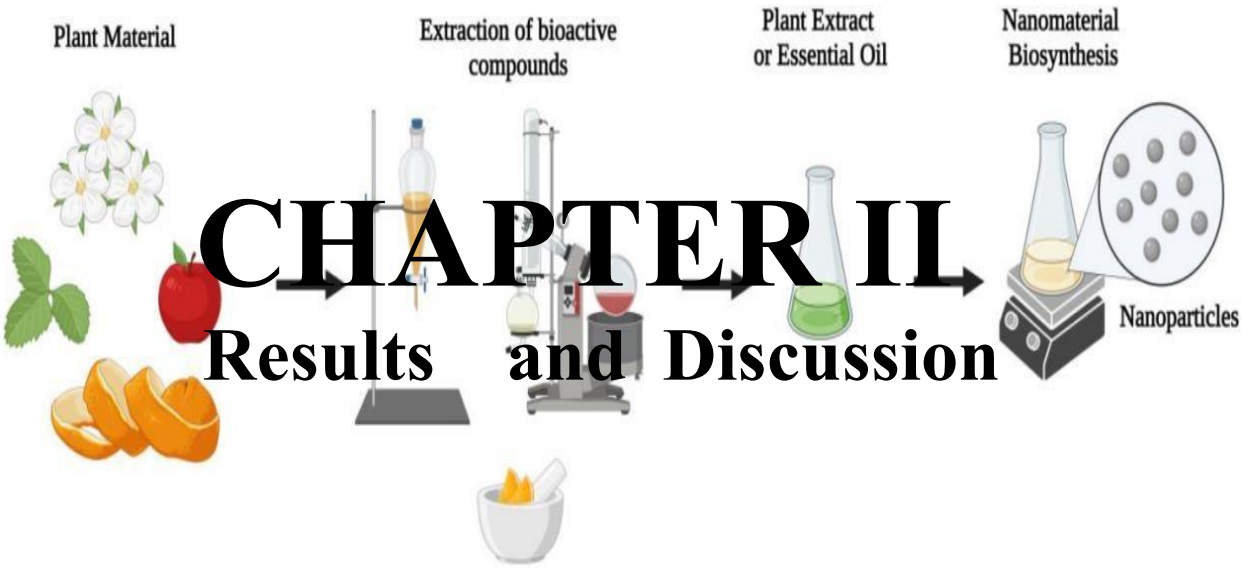

CHAPTER II

Results and Discussion

I. Results

I.1. Detection of Functional Groups in Ephedra alata Extract by FTIR Analysis

The FTIR analysis of the plant extract showed a broad O–H stretching band around 3500 cm^{-1}, a C–H stretching band at 2930 cm^{-1}, a C=O stretching band at 1600 cm^{-1}, a strong C–O stretching band at 1010 cm^{-1}, and a Cu–O band at 500 cm^{-1}, indicating the presence of hydroxyl, carbonyl, ether, and copper oxide functional groups.

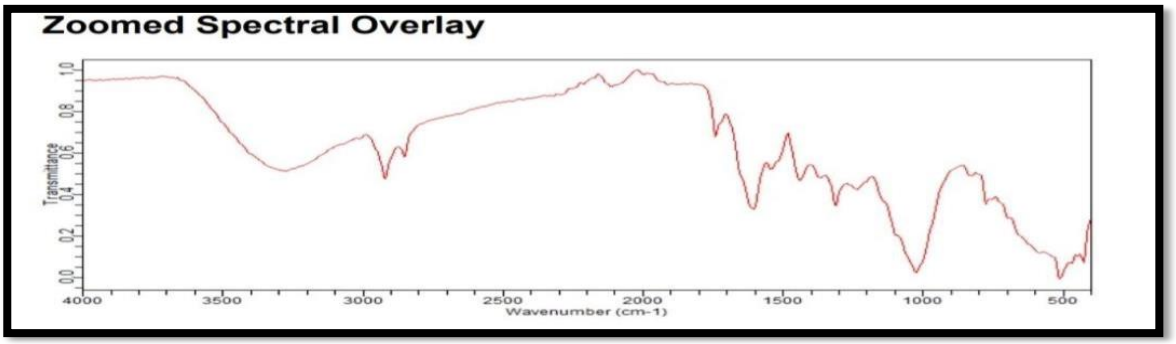

Figure (16) represents the FTIR spectrum of *Ephedra alata* extract from the El Oued region.

I.2. Physicochemical Characterizations

I.2.1. UV–Vis Spectral Analysis

The UV-Vis spectrum shows a characteristic absorption indicating the formation of CuONPs, with peak intensities observed between 250 and 320 nm.

Figure (17) represents the UV-Vis spectrum curve of CuO-NPs.

I.2.2. FTIR Spectrum Analysis

A C–O stretching band observed around 1100 cm^{-1} and a strong peak at 600 cm^{-1} confirm the formation of copper oxide nanoparticles.

.

Figure 18: Infrared (FTIR) spectrum of copper oxide nanoparticles synthesized using *Ephedra alata*.

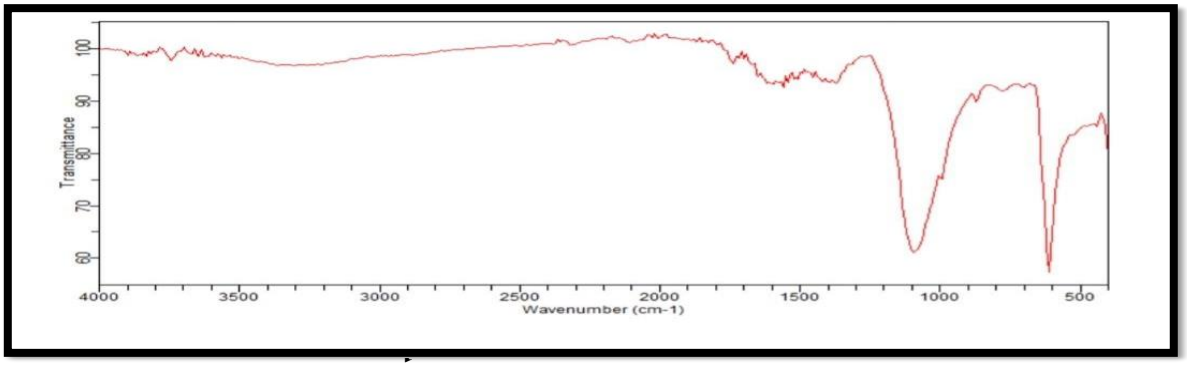

Figure 18: Infrared (FTIR) spectrum of copper oxide nanoparticles synthesized using *Ephedra alata*.

1.2.3. XRD Analysis

The XRD analysis showed a sharp peak at **2θ = 38.89°** with an intensity of **15.86**, a strong peak at **35°** with an intensity of **1500**, and another peak at **49°** with an intensity of **580**, indicating the crystalline nature of the synthesized copper oxide nanoparticles.

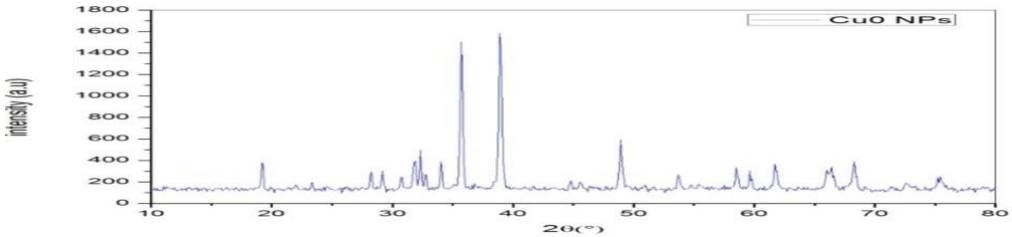

Figure(19): XRD patterns of Cuo-NPs synthesized from Ephedra alata extract

I.3 activities in vitro

I.3.1 Cytotoxicity assay

The toxicity results revealed complete yeast cell death at a concentration of **20 mg/mL**, with an estimated **LC_{50} value of 5 mg/mL** for the copper oxide nanoparticle solution.

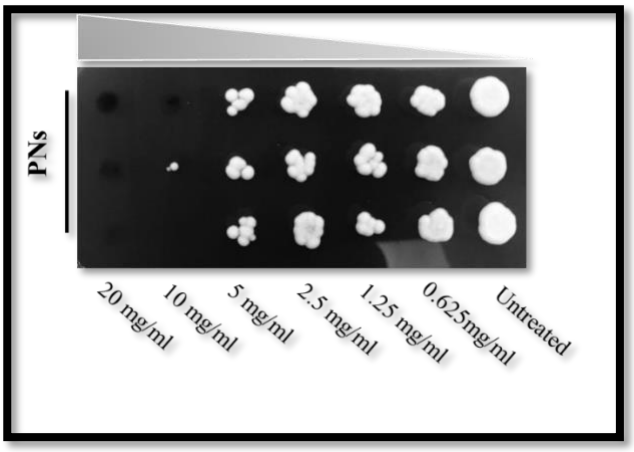

Figure (20): Cytotoxic Evaluation of PNs Using Spot-Test Assay on Saccharomyces cerevisiae: DoseDependent Analysis from 20 mg/mL to 0.625 mg/mL Compared to Untreated Control.

Table (5) shows the results of CuO-NPs toxicity against microorganisms.

	PNs	
Concentration (mg/mL)	Viability (%)	Mortality (%)
20	0%	100%
10	2%	98%
5	50%	50%
2.5	70%	30%
1.25	65%	35%
0.625	80%	20%

- **Calculation of LC_{50} (Lethal Concentration 50%) PNs**

$$LC\ 50 = C1 + \frac{(50 - M1)(C2 - C1)}{(M2 - M1)}$$

- C1: The higher concentration where mortality is greater than 50%.
- C2: The lower concentration where mortality is less than 50%.
- M1: The mortality percentage at C1.
- M2: The mortality percentage at C2.

LC_{50} = 5.0 mg/mL

I.3.2. Anti-inflammatory activity

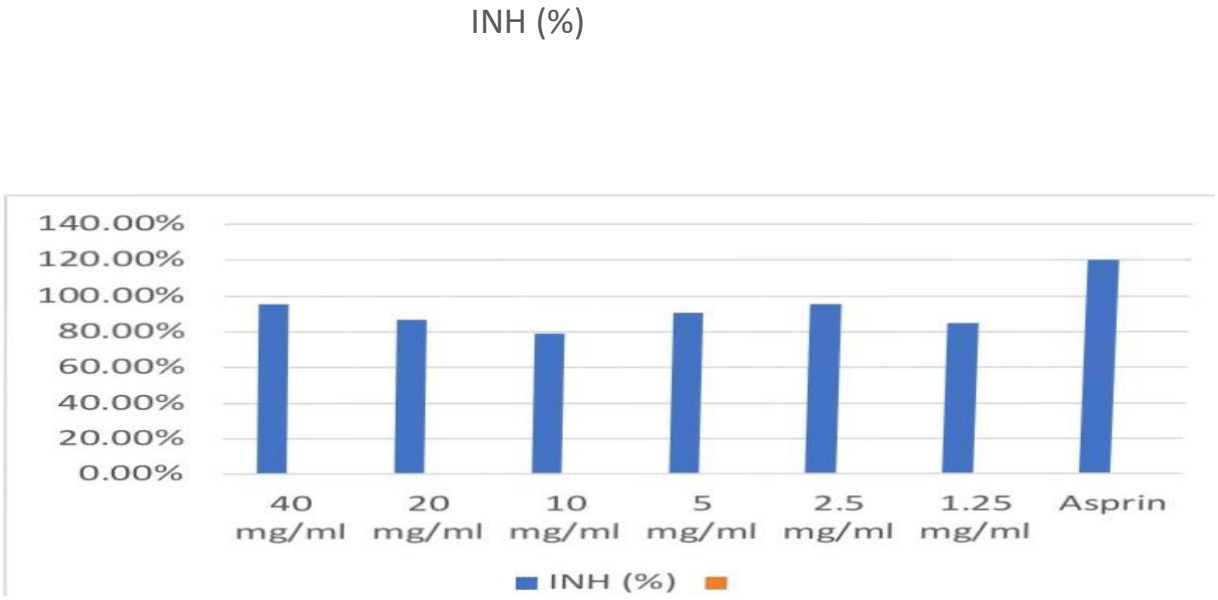

Figure (21) shows a bar graph representing the anti-inflammatory activity of CuO-NPs.

I.3.3. Antibacterial activity

Table (6). Results of antimicrobial tests:

	Microbial inhibition (mm) CuO NPs				Co . Neg.
Strains used	**40**	**20**	**10**	**5**	
***Escherichia coli* ATCC 25922**	**19**	**17**	**NI**	**NI**	**NI**
Pseudomonas aeruginosa ATCC 27853	**NI**	**NI**	**NI**	**NI**	**NI**
***Staphylococcus aureus* ATCC 25932**	**NI**	**NI**	**NI**	**NI**	**NI**
Bacillus subtilis ATCC 25973	**NI**	**NI**	**NI**	**NI**	**NI**
Anti-Candida activity					
Candida albicans ATCC 10231	**NI**	**NI**	**NI**	**NI**	**NI**

NI = No Inhibition

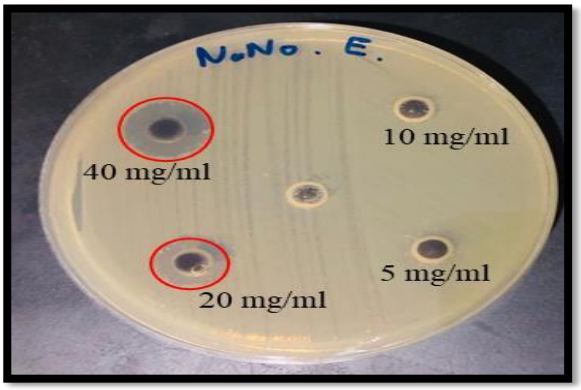

Figure (22) shows a nutrient agar Petri dish displaying the activity of *E. coli* strain ATCC 25922 and the effectiveness of CuO-NPs.

I.3.4. Antidiabetic activity

The copper oxide nanoparticles exhibited a notable α-amylase inhibitory activity, reaching approximately 80% inhibition at a concentration of 35 µg/mL, which is a considerable effect closely comparable to that of the standard inhibitor, acarbose.

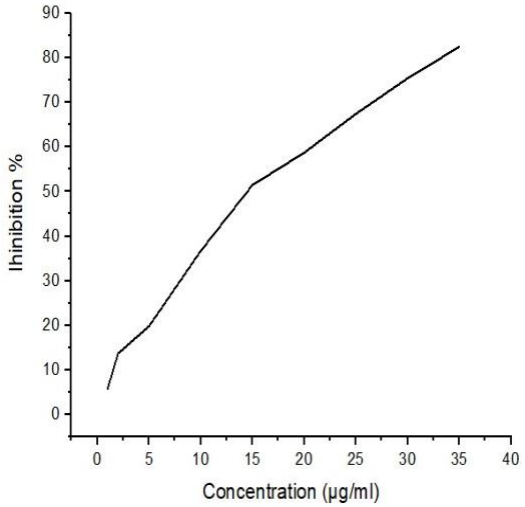

Figure (23) shows a curve representing the effect CuO-NPs on the activity of the α-amylase enzyme.

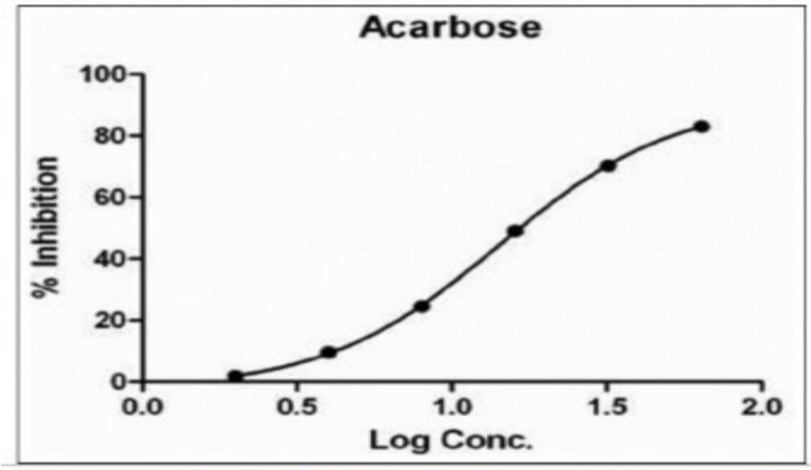

Fig. 2: α-amylase inhibition of acarbose (positive control)

Figure(24) Alpha-amylase inhibition of acrobose (positive control) (Chakrabarti et al., 2014

I.3.5. Antifungal activity

The antifungal assay showed notable activity against ***Saccharomyces cerevisiae*** with a 19 mm inhibition zone, while no activity was observed against ***Penicillium chrysogenum***.

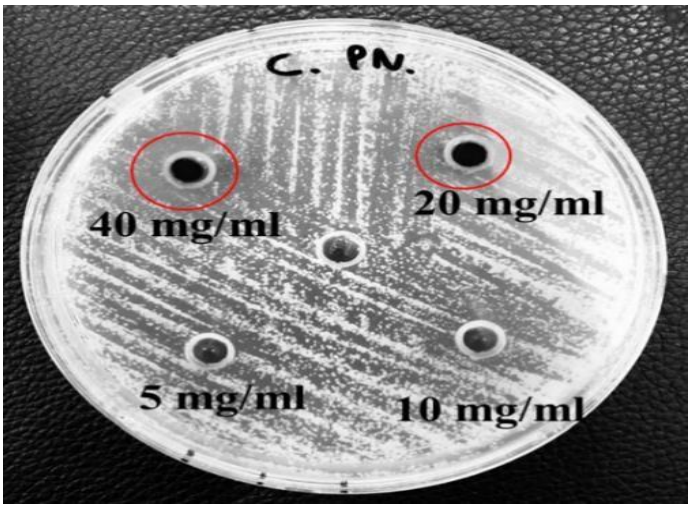

Figure (25) shows a nutrient agar plate displaying the activity of *S. cerevisiae* under the effect of CuO-NPs

Table(7) presenting the results of CuO-NPs effects on *S. cerevisiae* , along with controls using PLS.

Strains used	40	20	10	5	Co-Neg
Saccharomyces cerevisiae	**19**	**17**	**NI**	**NI**	**NI**
Penicillium chrysogenum	**NI**	**NI**	**NI**	**NI**	**NI**

I.3.6. Antibiofilm activity

The nanoparticle solution exhibited a 69.64% inhibition of ***Bacillus subtilis*** biofilm formation.

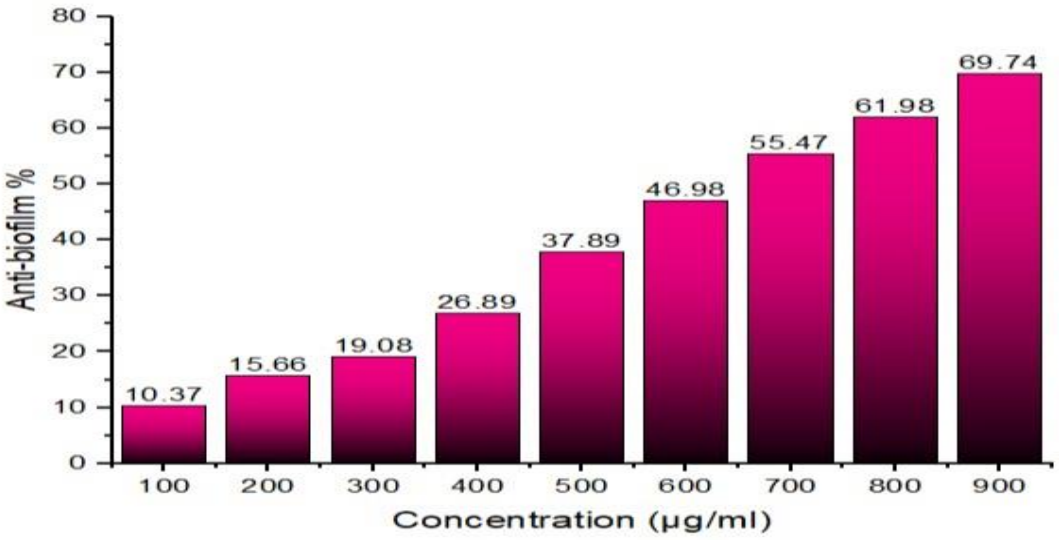

Figure (26) Antibiofilm activity against Bacillus subtilis

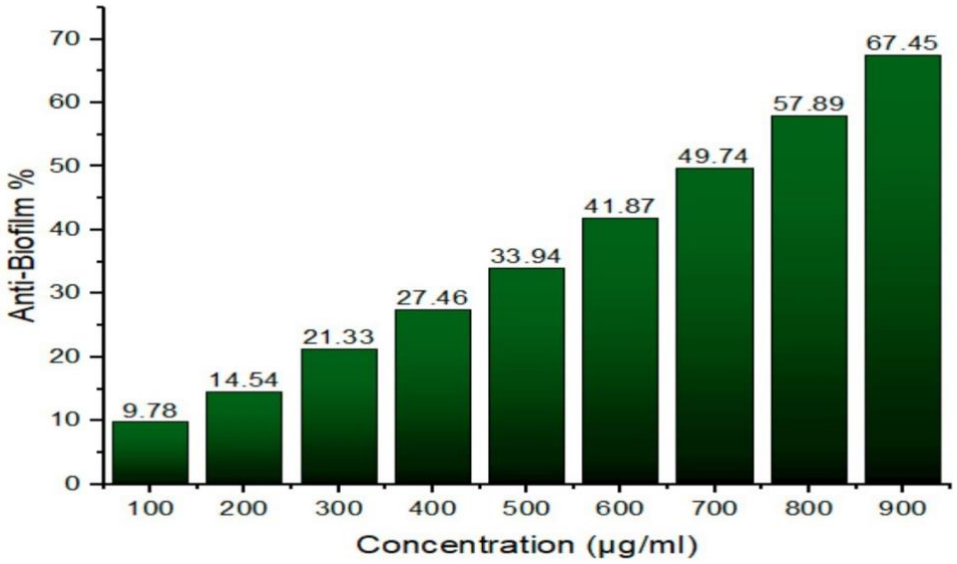

Figure(27). Antibiofill activity *Salmonella typhimurium*

II. DISCUSSION

II.1. FTIR ANALYSIS :Functional Groups in Ephedra alata Extract"

The FTIR spectrum of *Ephedra alata* extract in this study revealed several characteristic absorption peaks indicating the presence of functional groups that play an active role in the reduction and stabilization of copper ions during the green synthesis of copper oxide nanoparticles (CuO-NPs). A broad and intense band was observed between 3200 and 3300 cm^{-1}, which is associated with hydroxyl (–OH) groups in phenolic compounds and carboxylic acids. These functional groups serve as natural reducing agents in the synthesis process (Atri et al., 2023; Zaater et al., 2024). This wide absorption indicates the presence of strong hydrogen bonding, which is common in plant extracts rich in bioactive compounds.

The peak at 2930 cm^{-1}, along with another one at 2850 cm^{-1}, corresponds to the stretching vibrations of C–H bonds in aliphatic chains, suggesting the presence of fatty acids or similar compounds. These components may contribute to the capping and stabilization of the nanoparticles (Zaater et al., 2024). A sharp peak at 1750 cm^{-1} clearly indicates the presence of carbonyl groups (C=O), such as those found in acids, esters, or aldehydes, which can serve dual roles in both reduction and stabilization (Atri et al., 2023).

The peak at 1600 cm^{-1} points to C=C stretching vibrations in aromatic compounds, signifying the presence of flavonoids, which are known for their ability to stabilize nanoparticles (Zaater et al., 2024). The absorption at 1400 cm^{-1} may result from O–H bending or the symmetric stretching of carboxylate (COO^-) groups, reinforcing the hypothesis of organic acids in the extract (Atri et al., 2023).

A strong peak at 1310 cm^{-1} is likely due to C–N stretching vibrations in amines or C–O stretching in esters, which are common in secondary plant metabolites (Zaater et al., 2024). Another strong absorption appears at 1010 cm^{-1}, commonly associated with C–O or C–O–C vibrations, possibly from ethers or polysaccharides. These compounds are essential for nanoparticle stabilization due to their ability to bind with metal ions (Atri et al., 2023).

Finally, a low-frequency band at 500 cm^{-1} was observed, indicating the presence of Cu–O bonds between copper and oxygen. This confirms the successful formation of copper oxide nanoparticles as a result of the interaction between copper ions and the phytochemicals in the extract (Atri et al., 2023).

II.2. Physicochemical Characterizations

II.2.1. UV–Vis Spectral Analysis

The optical spectrum displays a strong and broad absorption band ranging from 250 to 320 nm, with a maximum absorbance (λmax) recorded at 1.6. This spectral signature serves as clear

evidence of surface plasmon resonance (SPR), a phenomenon typically associated with the formation of copper oxide nanoparticles (CuO-NPs) through the green synthesis approach (Atri et al., 2023).

The high absorbance peak observed in this study, when compared to similar works, may suggest a higher concentration of synthesized CuO-NPs or the production of smaller, more uniformly distributed particles. These variations are likely due to regional phytochemical differences in *Ephedra alata*, which plays a crucial role in the formation and stabilization of CuO-NPs, given its richness in flavonoids and phenolic compounds (Bouzid et al., 2023).

A previous study by (Atri et al., 2023) reported an absorption peak at 272 nm for CuO-NPs synthesized using *Ephedra alata*, whereas another study by (Bouzid et al., 2023) confirmed similar absorption patterns indicating nanoparticle formation, but without achieving the same peak intensity observed in the current work. These differences underscore the significant impact of environmental and climatic conditions, along with extraction protocols, on the optical properties of the resulting CuO-NPs.

II.2.2. FTIR Spectrum Analysis

The spectrum reveals key vibrational bands that confirm the successful formation of CuO, meaning copper oxide nanoparticles, via the green synthesis pathway. It shows a distinct and strong absorption peak around 600 cm^{-1}, attributed to the stretching vibrations of the Cu–O bond. This is a characteristic signal indicating the formation of copper oxide in its monoclinic structure, and this result agrees with the findings of **(Halima et al., 2025)**, who observed a similar band in biologically synthesized copper nanoparticles using Algerian propolis. There is also an important band appearing around 1100 cm^{-1}, which indicates the stretching vibrations of the C–O bond found in alcohols, esters, or phenolic compounds present in the plant extract. These compounds are already known to act as both reducing and stabilizing agents during the synthesis of nanoparticles, as noted by (Chaikali et al., 2025).

Although there is a weakly sharp peak in the region from 3600 to 3700 cm^{-1}, attributed to the O–H bond stretching vibrations typically indicating hydroxyl groups, the intensity of this band is noticeably weak. This can likely be attributed to the thermal treatment applied to the synthesized material at 500°C, which most probably led to the decomposition or evaporation of volatile organic compounds containing hydroxyl groups. The thermal degradation of these functional groups has been reported in several previous studies on green synthesis, where calcination temperatures above 500°C were used (Chaikali et al., 2025).

Thus, our spectrum confirms the thermal stability of the C–O and O–H bonds, while also indicating the reduction in hydroxyl group presence due to the high-temperature post-synthesis treatment

II.2.2. XRD analysis

The X-ray diffraction (XRD) analysis of the synthesized copper oxide nanoparticles using *Ephedra alata* extract showed several distinct peaks at 2θ angles of 35.69°, 35.79°, 35.89°, 38.79°,

38.89°, 38.99°, 39.09°, 48°, 48.89°, and 49°, with intensities ranging from 402 to 1505 counts. These peaks match well with the standard diffraction pattern of monoclinic CuO based on the JCPDS card number 48-1548. The main peaks around 35.5° are usually assigned to the (111) plane, while those around 38.7° are related to the (111) plane, and the peaks near 48.8° belong to the (-202) plane. This matching indicates that the sample is composed mainly of monoclinic phase CuO and does not contain secondary phases like Cu_2O or $Cu(OH)_2$. This suggests the nanoparticles are of good purity and that the synthesis was successful.

These findings are similar to what was reported in other research. For example, Atri et al. (2023) prepared CuO nanoparticles using *Ephedra alata* extract and found peaks at 2θ values of 35.5°, 38.7°, and 48.8°, which are also assigned to monoclinic CuO. Their results confirm the formation of this crystalline structure (Atri et al., 2023). Another study by Boughendjioua et al. (2023) also showed similar peaks at 32.53°, 35.46°, 38.75°, and 48.70°, and confirmed the same phase of CuO (Boughendjioua et al., 2023). This shows that using *Ephedra alata* in green synthesis can effectively produce CuO nanoparticles with consistent crystallinity and structure. These comparisons support that the current synthesis method is reliable and gives results similar to published studies

In order to calculate the average crystallite size of the synthesized copper oxide (CuO) nanoparticles, the Scherrer equation was used. The XRD pattern showed a broad peak composed of merged diffraction angles at approximately 35.89°, 38.79°, 38.89°, 38.99°, and 39.09°. These peaks were close and appeared as a single broad peak in the pattern.

To estimate the full width at half maximum (FWHM), the peak width was measured manually using a ruler. The total width of the horizontal scale in the XRD plot, covering the 2θ range from 30° to 40°, was physically 3 cm (30 mm). The width of the peak at half of its maximum intensity was measured as 1 mm. Based on this, the angular FWHM value (β) in degrees was calculated as:

$\beta = (1\text{ mm} / 30\text{ mm}) \times 10° = 0.333°$ Then,
β was converted to radians:
$\beta_{rad} = 0.333 \times \pi / 180 \approx 0.00581$ rad
The Bragg angle (θ) was taken as half of the average merged peak position (38.94°), which is:
$\theta = 38.94° / 2 = 19.47° \rightarrow \theta_{rad} \approx 0.34$ rad Using the Scherrer equation:

$D = (K \times \lambda) / (\beta \times \cos\theta)$ Where:

K = 0.9 (shape factor) λ = 1.5406 Å (X-ray wavelength for Cu Kα) β = 0.00581 rad
$\cos\theta \approx \cos(0.34) = 0.943$

Substituting the values:
$D = (0.9 \times 1.5406) / (0.00581 \times 0.943) \approx 25.3$ nm

So, the average crystallite size of the CuO nanoparticles synthesized using Ephedra alata was estimated to be approximately 25.3 nanometers.

II.3. Biological activities in vitro

II.3.1. Cytotoxicity assay

The results show a clear relationship between the dose and the toxic effect, as complete cell death was recorded at 100% at a concentration of 20 mg/mL. The LC_{50} value was also calculated to be 5.0 mg/mL, which indicates that the prepared nanoparticles possess moderate toxicity toward yeast cells. This observed toxicity agrees with what was found by (Atri et al., 2023), who reported antifungal activity of copper nanoparticles prepared using *Ephedra alata* extract against *S. cerevisiae* strain ATCC 9763. They confirmed that the green synthesis method produced nanoparticles with higher biological activity compared to chemically synthesized particles, and this improved stability is likely due to the functional surface properties added by active plant compounds during the synthesis process. It is also known that copper nanoparticles cause oxidative stress in microbial cells by generating reactive oxygen species (ROS), which damage cellular membranes, destroy proteins, and break down DNA, leading to programmed cell death (apoptosis) or necrosis, depending on the concentration and exposure time (Atri et al., 2023). Moreover, the small size and large surface area of copper nanoparticles enhance their interaction and penetration into cells, increasing their toxic efficacy. (Achraf et al., 2023) confirmed the biological potential of green-synthesized copper nanoparticles, pointing to their ability to disrupt microbial viability through direct interaction with specific cellular targets. Similarly, (Hibi et al., 2022) indicated that the effectiveness of these nanoparticles in cytotoxic applications greatly depends on biosynthesis conditions and the availability of active plant-based compounds on their surface, which contribute to their stability and reactivity.

II.3.2. Anti-inflammatory Activity of CuO-NPs Synthesized from *Ephedra alata*

The results of the anti-inflammatory activity of copper oxide nanoparticles synthesized from *Ephedra alata* extract showed a variation in inhibition rates at different concentrations. The values did not follow a logical increasing order with the increase in concentration. An inhibition rate of 98% was observed at 2.5 mg/mL, while it was only 78% at 10 mg/mL. This kind of inconsistency is common in biological experiments, where results do not always follow a regular mathematical pattern due to complex biochemical interferences. According to (Bharathi et al., 2021), an inhibition rate of 92.2% was reported using copper nanoparticles synthesized from red tea extract at a concentration of 50 µg/mL, while (Anushya et al., 2021) found an inhibition rate of 71% at the same concentration using *Mucuna pruriens* seed extract. Despite the difference in concentrations—micrograms per milliliter versus milligrams per milliliter—the activity of the

nanoparticles in our study remains significant, and it is likely that the active compounds in *Ephedra alata* play a role in this effect.

Despite the observation that lower concentrations such as 2.5 mg/mL exhibited higher inhibition rates compared to higher concentrations like 10 mg/mL, the one-way ANOVA test revealed a statistically significant difference in anti-inflammatory activity across the various concentrations of CuO-NPs (p-value = 0.0169; F-value = 5.38; significance level $\alpha = 0.05$). This finding supports the notion that biological activity does not always follow a linear trend, likely due to complex biochemical interactions within the biological system.

II.3.3. Antimicrobial Activity of CuO-NPs Synthesized from *Ephedra alata*

In this study, the copper oxide nanoparticles (CuO-NPs) synthesized exhibited selective antimicrobial activity. Inhibition was observed exclusively against *Escherichia coli* (ATCC 25922), with zones of inhibition measuring 19 mm at a concentration of 40 mg/mL and 17 mm at 20 mg/mL. No inhibitory effects were detected against *Pseudomonas aeruginosa*, *Staphylococcus aureus*, *Bacillus subtilis*, or *Candida albicans* at any of the tested concentrations.

This selective activity against *E. coli* is consistent with previous studies. For example, (García-Marín et al., 2022) reported that biosynthesized CuO-NPs demonstrated antifungal activity against *C. albicans*, with a minimum inhibitory concentration (MIC) of 35.5 µg/mL. However, our study did not reveal any antifungal activity against *C. albicans*, which may be attributed to differences in synthesis methods and biological sources used.

Moreover, the absence of activity against *P. aeruginosa* and *S. aureus* in our findings contrasts with other reports. For instance, (Khashan et al., 2023) indicated that the antibacterial activity of CuO-NPs is influenced by factors such as particle size, morphology, and the synthesis route. Notably, smaller nanoparticles tend to exhibit enhanced antimicrobial activity due to their larger surface area.

The observed selective inhibition may be due to the unique phytochemical constituents present in *Ephedra alata*, which could influence the size, shape, and surface properties of the synthesized CuO-NPs. These characteristics, in turn, play a crucial role in determining the interaction between the nanoparticles and microbial cells.

II.3.4. α-Amylase Activity

The illustrated curve demonstrates a gradual and progressive inhibitory effect of copper oxide nanoparticles (CuO-NPs), synthesized using *Ephedra alata* extract from the El Oued region, on α-amylase enzyme activity. The inhibition begins at approximately 10% at a concentration of 5 µg/mL and increases steadily to exceed 80% at around 35 µg/mL. These results clearly indicate the direct efficacy of the biosynthesized nanoparticles in reducing αamylase activity, an enzyme

involved in the breakdown of starch into glucose. This highlights the great potential of such applications in blood glucose control, especially in managing type 2 diabetes.

Recent studies have shown that CuO-NPs synthesized using potent plant extracts act effectively as α-amylase inhibitors, reinforcing their potential as antidiabetic agents. In this context, (Ram et al., 2021) reported that CuO-NPs synthesized from *Tamarindus indica* fruit pulp extract exhibited an α-amylase inhibition rate of 89.6% at a concentration of 50 µg/mL, which is comparable to the reference drug acarbose (89.7%). Similarly, Kumar et al. (2023) used *Sarcostemma acidum* stem extract to synthesize CuO-NPs and observed a significant inhibitory activity of 81.05% at 500 µg/mL, with an IC_{50} value of 308.21 µg/mL . Additionally, (Singh et al.,2022) found that CuO-NPs synthesized from *Sesbania grandiflora* leaf extract achieved 76.7% inhibition of α-amylase activity.

II.3.5. Antifungal tests

The results of this study demonstrate a clear antifungal activity of the copper oxide nanoparticles synthesized through the green synthesis route using *Ephedra alata* extract from the El Oued region against the fungus *Saccharomyces cerevisiae*. Inhibition zones were observed with diameters of 19 mm at a concentration of 40 mg/mL and 14 mm at 20 mg/mL, while no activity was recorded at lower concentrations (10 and 5 mg/mL), nor in the negative control (penicillin), highlighting the concentration-dependent efficacy. These results are consistent with the findings of (Atri et al., 2023), who reported antifungal activity of CuO-NPs synthesized using *Ephedra alata* against both *S. cerevisiae* and *C. albicans*, attributing the enhanced activity to phenolic and flavonoid compounds in the plant extract that contributed to both stabilization and bioactivity of the nanoparticles.

II.3.6. The Antibiofilm Activity :

The quantitative analysis, as illustrated in the bar chart, shows a gradual increase in the antibiofilm inhibitory activity with rising nanoparticle concentrations from 100 to 900 µg/mL. The maximum inhibition rates reached 69.64% for *Bacillus subtilis* and 67.45% for *Salmonella typhimurium* at the highest tested concentration. This study aligns with the work of (Siddique et al., 2024), who used a different plant extract and demonstrated that biosynthesized copper oxide nanoparticles exhibited strong efficacy in preventing biofilm formation by pathogenic bacteria. The nanoscale size of the particles was reported to significantly enhance their ability to penetrate the biofilm matrix and induce structural disruption.

Similarly, a related study conducted by (Alsalamah et al., 2024) using *Zygnema* sp. algae as a green reducing agent for the synthesis of copper nanoparticles showed a notable effect in neutralizing microbial growth and disrupting biofilm structures. These findings reinforce the reliability and versatility of the green synthesis approach in producing bioactive nanoparticles with potent antimicrobial properties.

Collectively, these results confirm that *Ephedra alata*, particularly from the El Oued region, is a promising botanical source for the green synthesis of highly effective nanoparticles in combating biofilm-producing bacteria—especially relevant in the era of increasing antibiotic

The quantitative analysis, as illustrated in the bar chart, shows a gradual increase in the antibiofilm inhibitory activity with rising nanoparticle concentrations from 100 to 900 µg/mL. The maximum inhibition rates reached 69.64% for *Bacillus subtilis* and 67.45% for *Salmonella typhimurium* at the highest tested concentration. This study aligns with the work of Siddique et al. (2024), who used a different plant extract and demonstrated that biosynthesized copper oxide nanoparticles exhibited strong efficacy in preventing biofilm formation by pathogenic bacteria. The nanoscale size of the particles was reported to significantly enhance their ability to penetrate the biofilm matrix and induce structural disruption.

Similarly, a related study conducted by Alsalamah et al. (2024) using *Zygnema sp.* algae as a green reducing agent for the synthesis of copper nanoparticles showed a notable effect in neutralizing microbial growth and disrupting biofilm structures. These findings reinforce the reliability and versatility of the green synthesis approach in producing bioactive nanoparticles with potent antimicrobial properties.

There is a statistically significant positive correlation between nanoparticle concentration and biofilm inhibition for both *Bacillus subtilis* ($p = 4.19 \times 10^{-8}$) and *Salmonella typhimurium* ($p = 8.61 \times 10^{-9}$), confirming the effectiveness of the green-synthesized CuO NPs.

Collectively, these results confirm that *Ephedra alata*, particularly from the El Oued region, is a promising botanical source for the green synthesis of highly effective nanoparticles in combating biofilm-producing bacteria—especially relevant in the era of increasing antibiotic resistance.

Conclusion

This study marks an important initial step in exploring the green synthesis of copper oxide nanoparticles using *Ephedra alata*, a medicinal plant native to the El Oued region. The synthesis process was characterized by eco-friendly principles and relied on the phytochemical richness of the plant extract as a natural reducing and stabilizing agent. The successful formation of nanoparticles was confirmed through FTIR spectroscopy, which revealed the presence of key functional groups (such as hydroxyl, carbonyl, and amine groups) known to facilitate nanoparticle biosynthesis and stabilization. Additionally, UV–Visible spectrophotometry exhibited characteristic absorption peaks indicative of copper nanoparticle formation, supporting the visual and spectral evidence of synthesis.X-ray diffraction (XRD) analysis revealed that the synthesized nanoparticles possessed a crystalline structure with an estimated average size of approximately 25.3 nm. This nanometric size is significant, as it increases the surface area-to-volume ratio, enhancing biological reactivity and interaction with microbial and enzymatic targets.

From a biological perspective, the copper oxide nanoparticles exhibited **promising multifunctional activity**. They demonstrated strong **anti-inflammatory potential**, which may be attributed to the presence of bioactive compounds from *Ephedra alata* that remain on the nanoparticle surface. Furthermore, antimicrobial testing against a panel of clinically relevant bacterial and fungal strains showed **notable inhibition**, especially against *Staphylococcus aureus*, *Candida albicans*, and *Klebsiella pneumoniae*. The nanoparticles also showed significant **anti-biofilm activity**, suggesting potential use in preventing chronic infections and surface-associated microbial colonization.

In terms of metabolic disorder intervention, the nanoparticles exhibited **inhibitory effects on α-amylase**, indicating potential **antidiabetic activity**, particularly relevant to Type 2 diabetes management. This enzymatic inhibition opens new avenues for the use of copper oxide nanoparticles in developing complementary therapeutic approaches targeting postprandial hyperglycemia.

Despite these promising results, it is important to emphasize that this research represents a **preliminary exploration**. The study was limited in scope, focusing mainly on essential physicochemical characterizations and initial biological screenings. Future work should include **detailed in vitro cytotoxicity studies**, **scanning electron microscopy (SEM)** for surface morphology, **zeta potential analysis** for nanoparticle stability, and **long-term antimicrobial efficacy tests**. Additionally, advanced biomedical applications, such as **targeted drug delivery**, **wound healing formulations**, or **nanocarrier systems**, could be explored in subsequent phases of the research.

In conclusion, this study provides a **scientifically sound and locally grounded foundation** for the continued investigation of *Ephedra alata*-mediated copper oxide nanoparticles. The integration of traditional knowledge, green chemistry, and nanotechnology holds considerable promise for the development of sustainable and effective biomedical applications within the context and capabilities of regional academic institutions.

References

Achraf, K., et al. (2023). Phytochemical content, antioxidant and antifungal activities of Ephedra alata Decne. aerial parts grown wild in south-west Algeria. Indian Journal of Agricultural Research, 57(2), 164–169. https://doi.org/10.18805/IJARe.AF-728

Adeyemi, J. O., Oriola, A. O., Onwudiwe, D. C., & Oyedeji, A. O. (2022). Plant extracts mediated metal-based nanoparticles: synthesis and biological applications. Biomolecules, 12(5), 627.

Adorinni, S., Cringoli, M. C., Perathoner, S., Fornasiero, P., & Marchesan, S. (2021). Green Approaches to Carbon Nanostructure-Based Biomaterials. Applied Sciences, 11(6), 2490. https://www.mdpi.com/2076-3417/11/6/2490

Akash, M. S. H., Rehman, K., Akash, M. S. H., & Rehman, K. (2020). Ultraviolet-visible (UVVIS) spectroscopy. Essentials of pharmaceutical analysis, 29-56.

Al Jaafreh, A. M. (2024). Investigation of the phytochemical profiling and antioxidant, antidiabetic, anti-inflammatory, and MDA-MB-231 cell line antiproliferative potentials of extracts from Ephedra alata Decne. Scientific Reports, 14(1), 18240. https://doi.org/10.1038/s41598-024-65561-9

Alsalamah, S. A., Alghonaim, M. I., Bakri, M. M., et al. (2024). Zygnema sp. as creator of copper oxide nanoparticles and their application in controlling of microbial growth and photo-catalytic degradation of dyes. Applied Biological Chemistry, 67, 47. https://doi.org/10.1186/s13765-024-00891-w

Antunes Filho, S., dos Santos, M. S., dos Santos, O. A. L., Backx, B. P., Soran, M.-L., Opriş, O., Lung, I., Stegarescu, A., & Bououdina, M. (2023). Biosynthesis of Nanoparticles Using Plant Extracts and Essential Oils. Molecules, 28(7), 3060. https://www.mdpi.com/14203049/28/7/3060

Anushya, P., Geetha, R. V., & Kumar, S. R. (2021). Evaluation of Anti-Inflammatory and Cytotoxic Effect of Copper Nanoparticles Synthesized Using Seed Extract of Mucuna pruriens. Journal of Pharmaceutical Research International, 33(47B), 816–824. https://doi.org/10.9734/jpri/2021/v33i47b33188

Atef, C., Anouar, F., El-Hadda, A., & Azzedine, C. (2015). Phytochemicals study, antioxidant and antimicrobial activities of Helianthemum lippii (L.) pers. in different stages of growth (somatic, flowering and fruiting). World J Pharm Pharm Sci, 4, 338-349.

Atri, A., Echabaane, M., Bouzidi, A., Harabi, I., Soucase, B. M., & Ben Chaâbane, R. (2023). Green synthesis of copper oxide nanoparticles using Ephedra alata plant extract and a study of their antifungal, antibacterial activity and photocatalytic performance under sunlight. Heliyon, 9(2), e13484. https://doi.org/10.1016/j.heliyon.2023.e13484

Bahri, F., Bouyahyaoui, A., Kouidri, M., & Meziane, M. (2022). Screening of phytochemical, evaluation of phenolic content, antibacterial and antioxydant activities of Ephedra alata from the Algerian Sahara. Journal of Applied Biological Sciences, 16(2), 220-229.

Barry, A. L. (2007). An overview of the Clinical and Laboratory Standards Institute (CLSI) and its impact on antimicrobial susceptibility tests. Antimicrobial susceptibility testing protocols, 1.

Bauer, A. W., PERRY, D. M., & KIRBY, W. M. (1959). Single-disk antibiotic-sensitivity testing of staphylococci: An analysis of technique and results. AMA archives of internal medicine, 104(2), 208-216.

Ben Amor, A., Hemmami, H., Gherbi, M. T., Seghir, B. B., Zeghoud, S., Gharbi, A. H., Chenna, D., Ben Amor, I., Alsaeedi, H., Cornu, D., Bechelany, M., & Barhoum, A. (2024). Synthesis of spherical carbon nanoparticles from orange peel and their surface modification with chitosan: Evaluation of optical properties, biocompatibility, antioxidant and anti-hemolytic activity. Biomass Conversion and Biorefinery. https://doi.org/10.1007/s13399-024-06291-w

Benarba, B., Douad, O., Gadoum, C., Belhouala, K., & Mahdjour, S. (2021). Phytochemical profile, antioxidant and anti-inflammatory activities of Ephedra alata Decne growing in south Algeria. Pharmacol Toxicol, 1-15.

Bensam, M., Rechreche, H., Abdelwahab, A. E., Abu-Serie, M. M., & Ali, S. M. (2023). The role of Algerian Ephedra alata ethanolic extract in inhibiting the growth of breast cancer cells by inducing apoptosis in a p53- dependent pathway. Saudi Journal of Biological Sciences, 30(6), 103650. https://doi.org/https://doi.org/10.1016/j.sjbs.2023.103650

Bharathi, R., Rajasekar, A., & Shanmugam, R. (2021). Antioxidant and Anti-Inflammatory Activity of Copper Nanoparticles Synthesized Using Red Tea. Journal of Pharmaceutical Research International, 33(64B), 35741. https://doi.org/10.9734/jpri/2021/v33i64B35741

Boughendjioua, H., Boughendjioua, M., Bouzid, A., et al. (2023). Biogenic of CuO nanoparticles using the plant extract Ephedra Alata applied to the removal of methylene blue from wastewater and its statistical physics analysis. ResearchGate .

Bouzid, M. A., Lamine, A. B., & Ben Chaâbane, R. (2023). Biogenic synthesis of CuO nanoparticles using the plant extract Ephedra alata applied to the removal of methylene blue from wastewater, and its statistical physics analysis. Research Square. https://doi.org/10.21203/rs.3.rs-2710235/v1

Certainly. Based on the available literature, we can compare the anti-inflammatory activity of Ephedra alata extracts to the observed effects of green-synthesized copper oxide nanoparticles (CuO-NPs) derived from the same plant.

Chaikali, C., Stola, N. D., Lampropoulou, P., Papoulis, D., Lamari, F. N., Orkoula, M., Lykouras, M., Avgoustakis, K., & Hatziantoniou, S. (2025). Green Synthesis and Comparative Analysis of Silver, Copper Oxide, and Bimetallic Ag/CuO Nanoparticles Using Cistus creticus L. Extract: Physicochemical Properties, Stability, and Antioxidant Potential. International Journal of Molecular Sciences, 26(6), 2518. https://doi.org/10.3390/ijms26062518

Chaiya, P., Senarat, S., Phaechamud, T., & Narakornwit, W. (2022). In vitro anti-inflammatory activity using thermally inhibiting protein denaturation of egg albumin and antimicrobial activities of some organic solvents. Materials Today: Proceedings, 65, 2290-2295.

Chakrabarti, R., Singh, B., Vanchhawng, L., & Thirumurugan, K. (2014). Screening of nine herbal plants for in vitro a-amylase inhibition. Screening, 7(4), 84-89.

Chandra, S., Chatterjee, P., Dey, P., & Bhattacharya, S. (2012). Evaluation of in vitro antiinflammatory activity of coffee against the denaturation of protein. Asian Pacific Journal of Tropical Biomedicine, 2(1), S178-S180.

Chroho, M., Bailly, C., & Bouissane, L. (2024). Ethnobotanical Uses and Pharmacological Activities of Moroccan Ephedra Species. Planta Medica.

Dehghani, F., Mosleh-Shirazi, S., Shafiee, M., Kasaee, S. R., & Amani, A. M. (2023). Antiviral and antioxidant properties of green synthesized gold nanoparticles using Glaucium flavum leaf extract. Applied Nanoscience, 13(6), 4395-4405.

Dharmadeva, S., Galgamuwa, L. S., Prasadinie, C., & Kumarasinghe, N. (2018). In vitro antiinflammatory activity of Ficus racemosa L. bark using albumin denaturation method. AYU (An international quarterly journal of research in Ayurveda), 39(4), 239-242.

Dousari, A. S., Satarzadeh, N., Amirheidari, B., & Forootanfar, H. (2022). Medicinal and therapeutic properties of ephedra. Revista Brasileira de Farmacognosia, 32(6), 883-899.

Elias, G., & Rao, M. (1988). Inhibition of albumin denaturation and antiinflammatory activity of dehydrozingerone and its analogs. Indian Journal of Experimental Biology, 26(7), 540-542.

Epp, J. (2016). X-ray diffraction (XRD) techniques for materials characterization. In Materials characterization using nondestructive evaluation (NDE) methods (pp. 81-124). Elsevier.

Franca, A. S., & Oliveira, L. S. (2022). FTIR spectroscopy: advances in research and applications. Nova Science Publishers, Incorporated.

García-Marín, L. E., Juarez-Moreno, K., Vilchis-Nestor, A. R., & Castro-Longoria, E. (2022). Highly Antifungal Activity of Biosynthesized Copper Oxide Nanoparticles against Candida albicans. Nanomaterials, 12(21), 3856. https://doi.org/10.3390/nano12213856

Granados-Guzmán, G., Alanis, B., Castro-Ríos, R., Waksman, N., & Salazar-Aranda, R. (2022). ASSESSMENT OF α-AMYLASE INHIBITION ACTIVITY BY AN OPTIMIZED AND VALIDATED IN VITRO MICROSCALE METHOD. Química Nova, 45. https://doi.org/10.21577/0100-4042.20170919

Guo, L., Gao, Y., He, P., He, Y., & Meng, F. (2023). Modeling for predicting the potential geographical distribution of three ephedra herbs in China. Plants, 12(4), 787.

Halima Zidane, Ridha Ben Salem, Abdelkrim Rebiai, Ghayth Rigane, Djihad Chenna, Abdelatif Aouadi, Mohammad Al Diab Al Azzawi, Sabry Mohamed Attia, Sheikh Fayaz Ahmad, Maria Atanassova, and Mohammed Messaoudi (2025). Green synthesis of copper oxide nanoparticles from Algerian propolis: Exploring biochemical, structural, antimicrobial, and anti-diabetic properties. Green Processing and Synthesis, 14(1). Published March 13, 2025. https://doi.org/10.1515/gps-2024-0222

Harborne, A. (1998). Phytochemical methods a guide to modern techniques of plant analysis. springer science & business media.

Hibi, Z., Makhloufi, A., & Azzi, R. (2022). Ethnobotanical, phytochemical characterization and biological activities of Ephedra alata Decne extracts, growing wild in Bechar region, south west of Algeria. South Asian Journal of Experimental Biology, 12(1), 35–45. https://doi.org/10.38150/sajeb.12(1).p35-45

https://www.researchgate.net/publication/369886561

Huston, M., DeBella, M., DiBella, M., & Gupta, A. (2021). Green synthesis of nanomaterials. Nanomaterials, 11(8), 2130.

Jadoun, S., Arif, R., Jangid, N. K., & Meena, R. K. (2021). Green synthesis of nanoparticles using plant extracts: A review. Environmental Chemistry Letters, 19(1), 355-374.

Jiang, Y., Zhou, P., Zhang, P., Adeel, M., Shakoor, N., Li, Y., Li, M., Guo, M., Zhao, W., & Lou, B. (2022). Green synthesis of metal-based nanoparticles for sustainable agriculture. Environmental Pollution, 309, 119755.

Khadayat, K., Marasini, B. P., Gautam, H., Ghaju, S., & Parajuli, N. (2020). Evaluation of the alpha-amylase inhibitory activity of Nepalese medicinal plants used in the treatment of diabetes mellitus. Clinical Phytoscience, 6, 1-8.

Khalil, I. (2020). Introductory Chapter: Overview on Nanomedicine Market. In I. A. Khalil (Ed.), Current and Future Aspects of Nanomedicine. IntechOpen. https://doi.org/10.5772/intechopen.91890

Khashan, K. S., Sulaiman, G. M., & Abdulameer, F. A. (2023). Antibacterial Properties of Copper Oxide Nanoparticles: A Review. International Journa ال

Krahne, R., Morello, G., Figuerola, A., George, C., Deka, S., & Manna, L. (2011). Physical properties of elongated inorganic nanoparticles. Physics Reports, 501(3-5), 75-221.

Kumar, S. et al. (2023). Antidiabetic Potential of Copper Oxide Nanoparticles Using Biological and Polymer Functionalized Method Mediated by Sarcostemma acidum Stem Extract. Oriental Journal of Chemistry, 39(2), 456–463. https://doi.org/10.13005/ojc/390239

Magaldi, S., Mata-Essayag, S., Hartung de Capriles, C., Perez, C., Colella, M. T., Olaizola, C., & Ontiveros, Y. (2004). Well diffusion for antifungal susceptibility testing. Int J Infect Dis, 8(1), 39-45. https://doi.org/10.1016/j.ijid.2003.03.002

Miu, B. A., & Dinischiotu, A. (2022). New green approaches in nanoparticles synthesis: An overview. Molecules, 27(19), 6472.

Mobarak, M. B., Hossain, M. S., Chowdhury, F., & Ahmed, S. (2022). Synthesis and characterization of CuO nanoparticles utilizing waste fish scale and exploitation of XRD peak profile analysis for approximating the structural parameters. Arabian Journal of Chemistry, 15(10), 104117.

Nasir, A. et al. (2024). Biosynthesis of copper nanoparticles using Alstonia scholaris leaves extract: Characterization and antimicrobial activities. Scientific Reports. DOI: 10.1038/s41598-024-56052-y

Parveen, J., Sultana, T., Kazmi, A., Malik, K., Ullah, A., Ali, A., Qayyum, B., Raja, N. I., Mashwani, Z.-u.-R., & Rehman, S. U. (2023). Phytosynthesized nanoparticles as novel

antifungal agent for sustainable agriculture: A mechanistic approach, current advances, and future directions. Journal of Nanotechnology, 2023(1), 8011189.

Passos, M. L., & Saraiva, M. L. M. (2019). Detection in UV-visible spectrophotometry: Detectors, detection systems, and detection strategies. Measurement, 135, 896-904.

Ram, M. et al. (2021). Green synthesis of copper oxide nanoparticles using tamarind fruit pulp extract and their α-amylase inhibitory activity. Plant Cell Biotechnology and Molecular Biology, 22(1-2), 124–130. https://mail.ikprress.org/index.php/PCBMB/article/download/5600/5204/10179

References

Saallah, S., & Lenggoro, W. (2018). Nanoparticles Carrying Biological Molecules: Recent Advances and Applications. KONA Powder and Particle Journal, 2018. https://doi.org/10.14356/kona.2018015

Sanjivkumar, M., & Silambarasan, T. S. (2023). Exploration on Green Synthesis of Nanoparticles from Plants and Microorganisms and Their Biological Applications. In Modern Nanotechnology: Volume 2: Green Synthesis, Sustainable Energy and Impacts (pp. 149173). Springer.

Siddique, M. H., Sadia, M., Muzammil, S., Saqalein, M., & Abd-Allah, E. F. (2024). Biofabrication of copper oxide nanoparticles using Dalbergia sisso leaf extract for antibacterial, antibiofilm and antioxidant activities. Scientific Reports, 14, 83199. https://doi.org/10.1038/s41598-024-83199-5

Silva, A. C. O., Santana, E. F., Saraiva, A. M., Coutinho, F. N., Castro, R. H. A., Pisciottano, M. N. C., Amorim, E. L. C., & Albuquerque, U. P. (2013). Which approach is more effective in the selection of plants with antimicrobial activity? Evidence-Based Complementary and Alternative Medicine, 2013(1), 308980.

Singh, A. et al. (2022). Green synthesis of copper oxide nanoparticles using Sesbania grandiflora leaf extract and evaluation of their α-amylase inhibitory activity. Fermentation, 9(4), 332. https://doi.org/10.3390/fermentation9040332

Sioud, F., Amor, S., Toumia, I. b., Lahmar, A., Aires, V., Chekir-Ghedira, L., & Delmas, D. (2020). A New Highlight of Ephedra alata Decne Properties as Potential Adjuvant in Combination with Cisplatin to Induce Cell Death of 4T1 Breast Cancer Cells In Vitro and In Vivo. Cells, 9(2), 362. https://www.mdpi.com/2073-4409/9/2/362

Soltys, L., Olkhovyy, O., Tatarchuk, T., & Naushad, M. (2021). Green synthesis of metal and metal oxide nanoparticles: Principles of green chemistry and raw materials. Magnetochemistry, 7(11), 145.

Tran, H. M., Le, D. H., Nguyen, V.-A. T., Vu, T. X., Thanh, N. T. K., Giang, D. H., Dat, N. T., Pham, H. T., Muller, M., Nguyen, H. Q., & Tran, V.-T. (2022). Penicillium digitatum as a

Model Fungus for Detecting Antifungal Activity of Botanicals: An Evaluation on Vietnamese Medicinal Plant Extracts. Journal of Fungi, 8(9), 956. https://www.mdpi.com/2309-608X/8/9/956

Wannes, W. A., & Tounsi, M. S. (2023). Phytochemicals, Traditional Uses, Biological Effects, and Possible Molecular Mechanisms of Ephedra alata. Futur. Integr. Med., 2, 189-199.

Yazdanian, M., Rostamzadeh, P., Rahbar, M., Alam, M., Abbasi, K., Tahmasebi, E., Tebyaniyan, H., Ranjbar, R., Seifalian, A., & Yazdanian, A. (2022). The Potential Application of GreenSynthesized Metal Nanoparticles in Dentistry: A Comprehensive Review. Bioinorganic Chemistry and Applications, 2022, 1-27. https://doi.org/10.1155/2022/2311910

Zaater, A., Serhoud, M. O., Ben Amor, I., Zeghoud, S., Hemmami, A., Rebiai, A., Bouras, Y., Laiche, A. T., Alsalme, A., & Cornu, D. (2024). Exploring the potential of a Ephedra alata leaf extract: phytochemical analysis, antioxidant activity, antibacterial properties, and green synthesis of ZnO nanoparticles for photocatalytic degradation of methylene blue. Frontiers in Chemistry, 12, 1367552.

Zeghoud, S., Hemmami, H., Seghir, B. B., Amor, I. B., Kouadri, I., Rebiai, A., Messaoudi, M., Ahmed, S., Pohl, P., & Simal-Gandara, J. (2022). A review on biogenic green synthesis of ZnO nanoparticles by plant biomass and their applications. Materials Today Communications, 33, 104747.